國立臺灣大學理學院大氣科學系
碩士論文
Department of Atmospheric Sciences
College of Science
National Taiwan University
Master's Thesis

理解反饋與熱量傳送對北極放大效應的貢獻
Understanding the Contributions of Feedbacks and Heat Transport to Asymmetric Arctic Amplification

周詩倪
SHIH-NI Zhou

指導教授：梁禹喬 博士
Advisor: YU-CHIAO Liang, Ph.D.

中華民國 113 年 12 月
December 2024

doi:10.6342/NTU202404648

致謝

感謝梁禹喬教授在各方面的指導與協助，不僅在研究上提供全然的支持、建議與學習機會，研究之餘也是很關心學生的師長，總能在百忙中撥出時間和每一位學生討論，面對我們各式各樣的問題也經常花時間一起想辦法。

我經常聽王逸說剛創立研究室時的各種事情，直到現在研究室已經有越來越多人；在我完成這份研究的期間，應數課也從無到有、越來越完整。無論是做研究或是完成任何一件事，小小的研究室讓我們特別都看得到作為指導教授付出的心力與重擔，謝謝禹喬不僅是這篇論文的指導教授，也是讓人敬重、學習的長輩。

同時感謝羅敏輝教授、黃彥婷教授與李時雨研究員作為口試委員撥冗協助完成研究；感謝所有極地氣候實驗室的同學與助理，一起窩在實驗室的小空間討論很多鬼點子，討論怎麼用最快的速度和最特別的方式慶祝教師節（連過教師節都要趕死線☺）、買好多奇怪的衣服過萬聖節、總會特別慶祝研究室位子被坐滿，還有很多細碎有趣的片段，很感謝待在研究室的每一天都有大家的幫助和陪伴。

2024.12

doi:10.6342/NTU202404648

中文摘要

北極放大效應指北極表面溫度變化幅度相較於全球其他區域更為顯著的現象，且在二氧化碳濃度降低和增加的情境下皆會出現，意指在二氧化碳減少造成全球冷卻的情境中，北極冷卻將比全球平均冷卻更顯著。本研究探討反饋交互作用對北極放大效應的影響，我們分析受到一系列廣泛的二氧化碳濃度（從工業化前的 1/8 倍到 8 倍）強迫的氣候模型模擬，結果表明北極放大效應確實在二氧化碳濃度下降的情況下發生，且冷卻北極放大效應的強度比二氧化碳濃度增加情境中的強度更強。反饋分析顯示，普朗克、失效率和反照率反饋是產生二氧化碳增加和減少情境中北極放大效應的主要因素，但與二氧化碳濃度減少最相關的是失效率反饋，其在冷卻情境中的強度比暖化情境中更強，不對稱的作用使得冷卻情境中有更強的北極放大效應。我們也藉由逐一關閉濕能量平衡模型中各項反饋，分析各反饋機制、大氣熱傳輸及其交互作用的貢獻。我們發現，在二氧化碳減少的冷卻模擬中，反饋交互作用對北極放大效應的貢獻比二氧化碳增加的模擬中的貢獻更強。特別的是，當二氧化碳濃度增加時，溫度垂直遞減率反饋的交互作用會導致負的北極溫度變化；而在二氧化碳濃度降低的情境下，則會產生正的溫度變化。這表明，溫度垂直遞減率反饋與其他反饋及大氣熱傳輸的交互作用是導致氣候冷卻情境下的北極放大效應比暖化情境更強的重要過程。反饋與大氣熱傳輸的交互作用通常會抵銷反饋間的交互作用。我們的結果突顯了非線性過程在產生北極放大效應對冷卻與暖化氣候不對稱反應中的重要性。

關鍵詞：冷北極放大效應；二氧化碳強迫；反饋鎖定；氣候反饋交互作用；非線性過程

doi:10.6342/NTU202404648

ABSTRACT

The Arctic amplification (AA), the phenomenon of amplified surface temperature response in the Arctic compared with the response elsewhere, can emerge under both reduced and increased carbon dioxide (CO2) forcings. In this study, we investigate the roles of feedback interactions contributing to AA. We analyze climate model simulations forced by a wide range of CO2 concentrations (from 1/8 to 8 times preindustrial level). Our results show that AA occurs not only under increasing CO2 but also under decreasing CO2, with the Arctic exhibiting an even stronger cooling-induced AA than the warming-induced counterpart. Moreover, the Planck, lapse-rate, and surface albedo feedbacks are identified as the primary contributors to AA in both scenarios. Among these, the lapse-rate feedback, in particular, demonstrates a stronger influence under CO2 reduction, thus reinforcing the asymmetric nature of AA in cooling versus warming climates. We also use a moist energy balance model (MEBM) to emulate the contributions of each feedback, atmospheric heat transport (AHT), and their interactions by locking the effect of each of them. We find that the contribution of feedback interactions to polar amplification is overall stronger in the CO2 reduction runs than in the CO2 increase runs. In particular, the lapse-rate feedback interaction in the CO2 increase runs leads to negative Arctic temperature change, whereas in the CO2 decrease runs leads to positive temperature change. This result indicates that the interaction of lapse-rate feedback and other feedbacks and AHT is a crucial process that gives rise to stronger AA in a cold climate state than that in a warm one. The feedback interaction with AHT generally counteracts the effect of feedback-feedback interactions. Our results highlight the importance of the nonlinear processes in producing AA asymmetric response to cooling and warming forcing agents.

doi:10.6342/NTU202404648

Keywords: cold Arctic amplification; CO2 forcing; feedback locking; climate feedback interactions; nonlinear processes

doi:10.6342/NTU202404648

CONTENTS

doi:10.6342/NTU202404648

LIST OF FIGURES

doi:10.6342/NTU202404648

doi:10.6342/NTU202404648

doi:10.6342/NTU202404648

Chapter 1 Introduction

Over the past 40 years, observational data indicate that near-surface air temperatures in the Arctic have risen between 2 to 4 times more rapidly than in other parts of the world (Serreze & Francis 2006, Serreze et al. 2009, Lenssen et al. 2019, Meredith et al. 2019, England et al. 2021, Chylek et al. 2022, Rantanen et al. 2022). This phenomenon, known as AA, has been widely attributed to elevated atmospheric CO2 levels (Manabe & Wetherald 1975, Gillett et al. 2008, Jones et al. 2013, Previdi et al. 2020, Taylor et al. 2022) and is projected to persist in the future (Long & Collins 2013). In addition, there is a vigorous debate focuses on whether the enhanced Arctic warming could influence extreme weather events and climate variability in the mid-latitudes of the Northern Hemisphere (Francis & Vavrus 2012, Barnes 2013, Cohen et al. 2014, Mori et al. 2014, Barnes & Screen 2015, Overland et al. 2015, 2016, Cohen et al. 2018, Coumou et al. 2018, Blackport et al. 2019, Blackport & Screen 2020a,b, Cohen et al. 2020, Zappa et al. 2021, Smith et al. 2022). Attention to AA extends beyond warming conditions and includes scenarios where CO2 levels diminish, potentially resulting in the Arctic cooling more pronounced than other regions. Therefore, understanding the AA under varying CO2 concentrations is crucial, as it has profound implications for the ecology and socioeconomics within the Arctic Circle, as well as for the dynamical changes in the global climate system.

While most studies have focused on AA under increasing CO2 concentrations, which can be simulated over century timescales (Pithan & Mauritsen 2014, Dai et al. 2019, Previdi et al. 2020, Hu et al. 2022, Liang et al. 2022a), less is known about AA under cooling scenarios. In these scenarios, Arctic cooling is expected to be more pronounced

doi:10.6342/NTU202404648

than cooling in other regions of the globe. Recent studies examining how aerosol emissions affect global and Arctic climates suggest that AA can also emerge under cooling influences (Jiang et al. 2020, England et al. 2021). On the other hand, paleo-climate investigations have revealed that AA patterns manifest during both CO2 decreases and increases. For instance, Hoffert & Covey (1992) and Miller et al. (2010) assessed AA's magnitude during climatic intervals such as the Holocene Thermal Maximum, Last Glacial Maximum, Last Interglacial, and mid-Pliocene periods using paleo-climate proxies. Nevertheless, these studies have not yet comprehensively compared the mechanisms of AA under both cooling and warming scenarios, nor have they contrasted the phenomenological and mechanistic differences between cooling driven and warming-driven AA.

In climate change research, the timescale required for the climate system to reach equilibrium in response to greenhouse gas forcing is often overlooked. Although previous studies have suggested that the climate system gradually reaches equilibrium over timescales ranging from hundreds to thousands of years (Dai et al. 2020, Dunne et al. 2020, Rugenstein et al. 2020), most current coupled model intercomparison projects still focus on simulations spanning 150 years, such as Phase 6 of the Coupled Model Intercomparison Project (CMIP6). For example, CMIP6 uses a 150-year abrupt fourfold CO2 experiment to estimate equilibrium climate sensitivity (Eyring et al. 2016). However, such simulation durations may be insufficient to fully capture the nonlinear feedback mechanisms during long-term climate change, especially those involving dynamic feedbacks in the Arctic and other high-latitude regions. Long-term simulations by Rugenstein et al. (2020) show that as the simulation duration extends to 1000 years, the global average temperature increase is significantly higher than that estimated from the first 150 years. Our findings indicate that the response of Northern Hemisphere surface

doi:10.6342/NTU202404648

warming is nearly 500 years faster than that of cooling. Our study attempts to compare the feedback mechanisms between the first and last 150 years of a 1000-year simulation, which could greatly reveal the extent to which specific mechanisms are directly or indirectly influenced by the long timescales required for ocean heat transport equilibrium (Yang & Zhu, 2011). Studies by Jansen (2017) and Yang & Zhu (2011) emphasize that oceanic vertical mixing and heat transport are crucial for near surface temperature responses in high northern latitudes. In particular, Jansen (2017) highlights the direct relationship between atmospheric cooling or warming and changes in deep ocean circulation and stratification. Chalmers et al. (2022) further connects these response time differences in high-latitude regions to the advance and retreat of sea ice and the associated amplified lapse-rate feedback and surface albedo feedback timing. This study will not only enhance our understanding of the dynamics of feedback mechanisms in the Arctic under different simulation durations but also provide a new perspective for examining Arctic feedback mechanisms, leading to a more comprehensive understanding of the long-term changes in the climate system under varying conditions.

Recently, the traditional feedback analysis framework has been expanded to study regional warming driven by spatially varying feedbacks (Armour et al. 2013, Pithan & Mauritsen 2014). Some studies have investigated the contribution of each climate feedback to Arctic Amplification, identifying that the lapse-rate feedback contributes the most to Arctic Amplification, followed by changes in the Planck feedback and surface albedo feedback (Pithan & Mauritsen 2014, Stuecker et al. 2018, Goosse et al. 2018). Although water vapor feedback is ubiquitous, it is strongest in low-latitude regions and contributes more to tropical warming than to Arctic warming, thus acting as a primary factor that mitigates Arctic Amplification. Analyzing regional warming through the spatial structure of feedbacks provides a computationally efficient approach and allows

doi:10.6342/NTU202404648

for a clean decomposition of surface warming, as the sum of the warming contributions from individual feedbacks equals the total warming. However, this method does not account for changes in AHT associated with the strength of individual feedbacks, which can affect regional warming and potentially influence Arctic Amplification (Langen et al. 2012, Russotto & Biasutti 2020). Therefore, the traditional feedback analysis framework may lack sufficient interpretation of the interactions between feedbacks and AHT when attributing the Arctic Amplification effect.

Another approach to evaluating the impact of specific climate feedbacks is feedback locking. This method involves "locking" a particular feedback within a model—holding it artificially constant—and then assessing how the climate system responds to perturbations when that feedback no longer adapts. The logic behind this approach is that no feedback operates in isolation: they interact with one another as well as with the broader climate system, particularly through mechanisms such as AHT. By comparing scenarios in which a given feedback is locked versus fully active, we can attribute changes in surface warming to that feedback and examine how other processes compensate. For example, studies have locked surface albedo feedback and found that even though it strongly influences polar amplification, its net effect on global mean temperature is modest (Hall 2004, Graversen & Wang 2009). Furthermore, work has shown that AHT can compensate for a locked feedback, allowing the climate to maintain a warming pattern comparable to scenarios where all feedbacks freely adjust (Langen et al. 2012). These compensations highlight the interconnected nature of feedbacks and processes: when one feedback is altered, water vapor transport and other feedbacks shift to reach a new equilibrium. Consequently, the warming attributed to individual feedbacks does not simply sum to the total warming because other parts of the system respond dynamically to changes in feedback strength, especially AHT (Russotto & Biasutti 2020).

doi:10.6342/NTU202404648

In this study, we combine radiative kernel techniques with a MEBM to disentangle these complex interactions and quantify the contributions of various radiative feedbacks and their coupled processes to Arctic Amplification. The MEBM framework allows us to hold certain surface flux conditions fixed, ensuring that any resulting adjustments in the climate system, including shifts in feedback distributions and atmospheric heat transport, are clearly linked to the feedbacks themselves. By performing feedback locking experiments within the MEBM, we can observe how changing one feedback alters the meridional structure of moist static energy, modulates atmospheric heat transport, and influences other feedbacks in turn. This approach goes beyond traditional methods by revealing how each feedback's role in Arctic Amplification is not an isolated property, but rather the outcome of a delicate balance among radiative processes, surface heat fluxes, and large-scale energy transports.

Our findings show that the Arctic's characteristic lapse-rate feedback, commonly viewed as closely tied to sea ice and surface albedo changes, is actually intertwined with the distribution of atmospheric energy. In high-latitude regions where vertical convection is relatively weak, energy convergence by AHT can amplify or counteract certain feedbacks. Changes in the vertical temperature structure translate into distinct positive or negative lapse-rate feedbacks, depending on the latitude and the relative strength of surface and upper-atmospheric warming. The interaction between feedback locking and MEBM simulations shows how changes in the vertical temperature structure, along with changes in horizontal heat transport, affect where and how Arctic Amplification takes place. In other words, while surface and radiative feedbacks are important drivers of Arctic warming, their overall effect depends on how the entire climate system, especially atmospheric heat transport, adjusts and responds to them. This way of understanding feedback processes suggests that Arctic Amplification cannot be fully

doi:10.6342/NTU202404648

explained by local sea ice changes alone. Instead, it comes from the combined effects of multiple feedbacks and large-scale energy flows working together.

High-latitude lapse-rate feedback makes a significant contribution to AA under cooling scenarios. According to the method of Feldl et al. (2020), these feedbacks are primarily divided into “upper” and “lower” contributions. This distinction is derived from the separation of the high-latitude troposphere from other parts of the atmosphere by the characteristic climatic isotropic surface. This decomposition clarifies that the positive high-latitude lapse-rate feedback over polar oceans mainly arises as an atmospheric response to regional sea ice loss, while it decreases in subpolar latitudes due to increased poleward energy transport. Lapse-rate feedback manifests as negative feedback in low-latitude regions, mainly driven by moist convection, which causes more pronounced warming of the upper troposphere, increasing outgoing longwave radiation and thereby offsetting further surface warming. Notably, most studies have concentrated on warming scenarios, leaving cooling cases less explored. By distinguishing regional drivers of high-latitude lapse-rate feedback, we gain insights into its interaction with non-local processes such as heat transport and surface heat flux, further influencing Arctic Amplification.

We also analyze the regional and remote contributions of high-latitude lapse-rate feedback following Feldl et al. (2020). This approach decomposes the feedback into components associated with different atmospheric layers defined by the 285-K isotherm, allowing us to isolate surface-driven processes, such as ocean-to-atmosphere energy transfer linked to sea ice extent changes (Deser et al. 2015, Blackport & Kushner 2017, Oudar et al. 2017, Dai et al. 2019) or albedo feedback (Graversen et al. 2014, Feldl et al. 2017, 2020), from those involving atmospheric convection and heat transport. Poleward atmospheric heat transport, which warms the upper troposphere at high latitudes (Alexeev et al. 2005, Caballero & Langen 2005, Hwang et al. 2011, Alexeev & Jackson 2013),

doi:10.6342/NTU202404648

supports a negative upper-level lapse-rate feedback. A clearer understanding of how changes in CO2 concentrations affect AA will help improve the representation of high-latitude feedback mechanisms in climate models and provide valuable insights into the nonlinear characteristics of feedback interactions within the climate system.

Understanding how changes in CO2 concentrations influence AA is crucial for gaining a more complete view of how the climate system responds, particularly in polar regions. The primary objectives of this study include:

(i) Comparing AA under scenarios of increased and decreased CO2, identifying and quantifying the contributions of key feedback mechanisms to AA.

(ii) Identifying and quantifying the contributions of various feedbacks to AA under reduced CO2 conditions through feedback locking experiments.

(iii) Discussing how interactions among feedback mechanisms and AHT influence the strength of AA, revealing asymmetric responses between cooling and warming scenarios.

doi:10.6342/NTU202404648

Chapter 2 Data and Methods

2.1 Feedback Analysis using Radiative Kernels

This study examines a series of fully coupled atmosphere-ocean-sea ice-land simulations under various abrupt CO2 forcings levels (Mitevski et al. 2021, 2022). We use the Community Earth System Model version 1 (CESM1, Kay et al. 2015), which incorporates the Community Atmosphere Model version 5 (CAM5), the Community Ice CodE version 4 (CICE4), the Community Land Model version 4 (CLM4), and the Parallel Ocean Program version 2 (POP2), all using a horizontal resolution of 1 degree. Our experiments consist of both enhanced and reduced CO2 concentrations relative to preindustrial (PI) levels, specifically 0.125x, 0.25x, 0.5x, 1x (PI), 2x, 3x, 4x, 5x, 6x, 7x, and 8x PI CO2. During all runs, the concentrations of other trace gases, ozone, and aerosols are held constant at their PI values. Following the CMIP6 4xCO2 protocol (Eyring et al. 2016), each simulation is initialized from PI conditions and integrated for 150 years. We define the response of any variable as the difference between each nxCO2 experiment and the 1xCO2 control, denoted as Δ, and use the final 30 years to represent the equilibrium response. Additionally, we extend the existing 150-year instantaneous 2xCO2 and 0.5xCO2 simulations to 1000 years to investigate feedback asymmetry over longer periods.

To quantify the strength of AA, we define a dimensionless Arctic Amplification Factor (AAF) as:

$$AAF = \frac{\Delta SAT_{Arctic}}{\Delta SAT_{global}}$$

where ΔSAT_{Arctic} is the Arctic (60°-90°N) mean surface-air temperature response, and

doi:10.6342/NTU202404648

ΔSAT_{global} is the global mean SAT response. This definition of AAF has been widely used, and its physical interpretation has been discussed in many studies involving abrupt CO2 experiments on AA (Pithan & Mauritsen 2014, Goosse et al. 2018, Liang et al. 2022a).

To explore the drivers behind AA, we perform a feedback decomposition using the Arctic (60°-90°N) and tropical (30°S-30°N) top-of-atmosphere (TOA) energy budgets (Soden et al. 2008). The basic atmospheric energy budget relation can be expressed as:

$$\Delta R + \Delta F - \Delta H_o = 0$$

Here, ΔR is the response of net downward radiation at the TOA, ΔF is the response of the horizontal convergence of atmospheric and oceanic energy transport, and ΔH_o is the ocean heat uptake response. The contribution from ocean heat storage dominates over the negligible heat capacity of the atmosphere, land, and snow/ice melt (Polvani et al. 2020, Liang et al. 2022b). We infer ΔF as the residual between ΔR and ΔH_o. Following previous work (Pithan & Mauritsen 2014, Polvani et al. 2020, Hahn et al. 2021, Jenkins & Dai 2021, Beer & Eisenman 2022, Liang et al. 2022b, Wu et al. 2023), we separate ΔR into contributions from the Planck response (ΔR_{PL}), the lapse-rate response (ΔR_{LR}), the albedo response (ΔR_{ALB}), the water vapor response (ΔR_{WV}), and the cloud response (ΔR_{CLD}). We use radiative kernels from CAM5 (Pendergrass et al. 2018) to accomplish this decomposition. The effective radiative forcing (ERF), ΔR_F, is determined using a corresponding set of fixed-SST simulations that vary CO2 and by taking the 30-year average change in TOA energy flux (Mitevski et al. 2021).

$$\Delta R = \Delta R_F + \Delta R_{PL} + \Delta R_{LR} + \Delta R_{ALB} + \Delta R_{WV} + \Delta R_{CLD}$$

Next, ΔOHT (the oceanic heat transport response) is derived as the difference between ΔH_o and the change in net surface heat flux (shortwave, longwave, latent, and sensible) between ocean and atmosphere. The atmospheric heat transport response (ΔAHT) then follows as the difference between ΔF and ΔOHT.

doi:10.6342/NTU202404648

All terms are converted into corresponding temperature changes by dividing by the negative global mean Planck feedback parameter ($-\lambda_0$), as described by Pithan & Mauritsen (2014) and Goosse et al. (2018). Any residual in the radiative kernel approximation is determined by comparing the total TOA radiation response to the sum of these individual feedback contributions. In general, this residual tends to be small compared to the other components.

2.2 Feedback Locking Analysis

This study employs the MEBM configuration described in Beer & Eisenman (2022) to simulate changes in surface temperature and AHT under various CO2 forcings. The MEBM is a simplified climate model that emphasizes horizontal energy transport, assuming heat primarily diffuses within the atmosphere. We conducted feedback locking experiments by fixing specific feedback parameters within the MEBM framework to analyze the warming response in the absence of those feedbacks. In these experiments, we quantified changes in surface temperature due to individual locked feedbacks by comparing results from scenarios with all feedbacks active against those where one feedback was locked.

The MEBM approximates AHT as a diffusion process involving surface temperature and specific humidity, capturing temperature and AHT changes similar to comprehensive climate models while maintaining computational efficiency (Bonan et al. 2018, Armour et al. 2019). Numerous studies have established MEBM's utility in evaluating individual radiative feedbacks' impact on temperature and AHT under global warming (Hwang & Frierson 2010, Rose et al. 2014, Roe et al. 2015, Russotto & Biasutti 2020). By incorporating latent heat effects from atmospheric water vapor transport, MEBM builds

doi:10.6342/NTU202404648

on a dry energy balance model framework, providing a more accurate depiction of AHT dynamics, particularly in high-latitude regions.

In our feedback locking analysis, simulations were conducted for each feedback locking scenario to assess their temperature contributions. To "lock" a specific feedback within this framework, Beer & Eisenman (2022) modify the original TOA energy budget equation by removing the contribution of that feedback. This is achieved mathematically by adjusting the feedback parameter λ_i for the targeted feedback, as shown in the modified energy budget equation:

$$(\lambda - \lambda_i)\,\Delta T_{-i} + \Delta R_F + \Delta F - \Delta H_o = 0$$

where T_{-i} denotes the temperature response when the feedback λ_i is locked. Total warming T depends nonlinearly on λ, as discussed by Roe & Baker (2007). Locking a feedback fixes the temperature change associated with that feedback, while interactions among feedbacks modify the overall warming response. Each feedback influences AHT, adjusting according to regional warming changes induced by other feedbacks.

By solving this equation, we isolate the temperature contribution due solely to the locked feedback, ΔT_i, by taking the difference between the total warming and the temperature response with the locked feedback:

$$\Delta T_i = \Delta T - \Delta T_{-i}$$

For further accuracy in describing feedback interactions, the warming contributions due to feedback locking can be separated into three components: direct warming from individual feedback, interactions among feedbacks, and interactions between feedbacks and AHT. This means that the influence of an individual feedback on temperature not only directly affects the climate system but also modifies the response of other feedbacks through changes in total warming and AHT. This approach allows us to effectively distinguish the direct contributions of individual feedbacks from all other nonlinear

doi:10.6342/NTU202404648

interactions.

$$\Delta T_i = \lambda_i \frac{\Delta T}{-\lambda_0} + \frac{\sum_{i \neq j} \lambda_j \Delta T_i}{-\lambda_0} + \frac{\Delta F - \Delta F_{-i}}{-\lambda_0}$$

doi:10.6342/NTU202404648

Chapter 3 Results

3.1 Asymmetric Climate Response under CO2 Forcing

We first examine the time series of annual mean SAT over the Arctic and the globe throughout the 150-year simulations (Figure 1a). As expected in abrupt CO2 experiments, both Arctic and global SATs adjust rapidly during the first 30 years before gradually approaching a quasi-equilibrium state. Correspondingly, sea ice extent (SIE) either expands or contracts in response to the forcing (Figure 1b). For instance, under 7x and 8xCO2, the sea ice melts rapidly within the first 15 years, resulting in an ice-free Arctic thereafter, whereas lower CO2 scenarios produce a slow but steady growth in SIE. The degree of sea ice response reflects the intensity of the CO2 forcing. Throughout the 150-year integration, the AAF is consistently larger under reduced CO2 conditions than under elevated CO2 conditions (Figure 1c). This outcome, which may seem unexpected, highlights an inherent asymmetry in the intensity of AA between scenarios of increasing versus decreasing CO2 levels.

doi:10.6342/NTU202404648

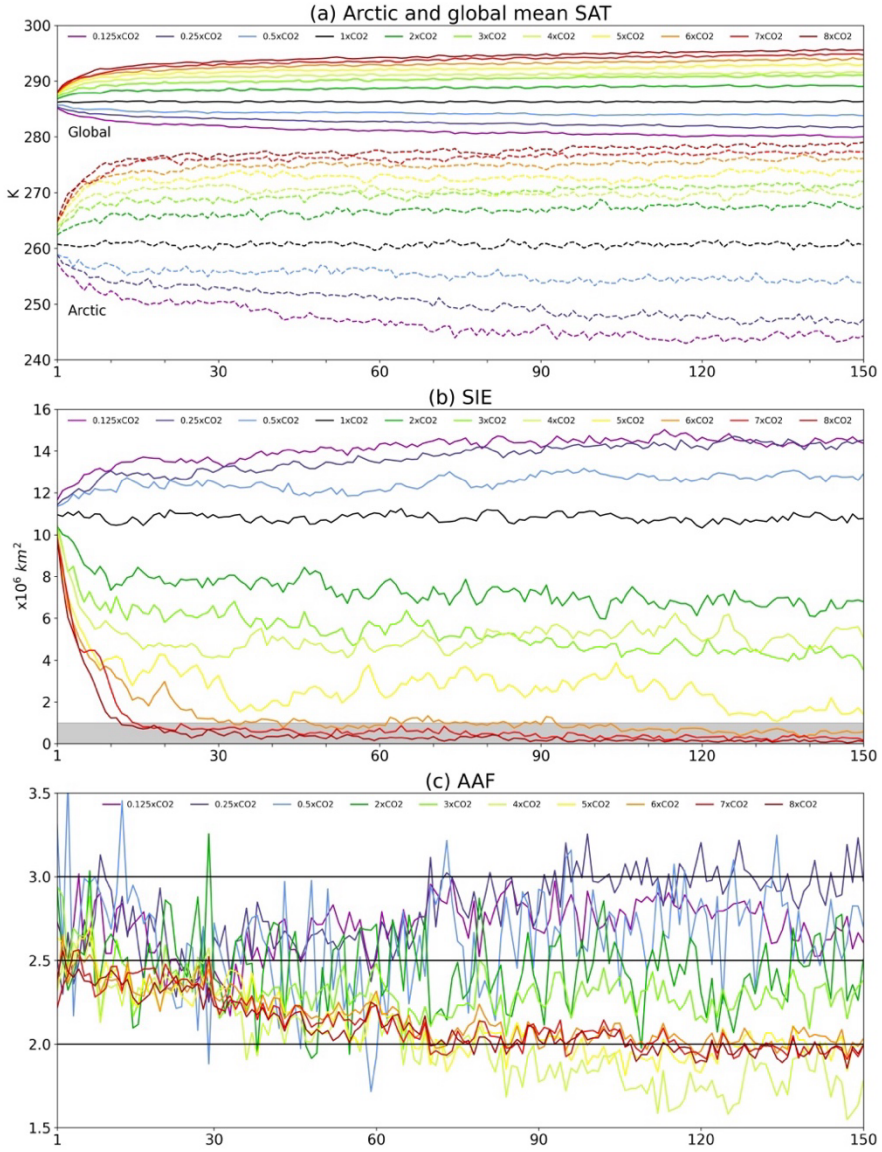

Figure 1: (a) Annual-mean Arctic and global mean SAT time series for each nxCO2 experiment. (b) and (c) Same as in (a), but showing annual-mean Arctic SIE and AAF, respectively. The gray shaded area in (b) denotes ice-free conditions, defined as SIE falling below 1,000,000 square kilometers.

doi:10.6342/NTU202404648

We then examine the mean responses of Arctic SAT, SIE, and turbulent heat flux over the final 30 years to illustrate their coupling relationships and reveal the mechanisms under varying CO2 forcing intensities. These variables exhibit consistent patterns of variation with CO2 forcing intensity and are strongly interrelated (black lines in Figures 2a-c). This alignment reflects a well-established feedback process: as CO2 increases, Arctic SAT rises, accelerating sea ice melt and exposing more open water, thus enhancing ocean-atmosphere heat exchange (Deser et al. 2010, Screen & Simmonds 2010, Goosse et al. 2018, Dai et al. 2019, Liang et al. 2022a). The same feedback loop operates when CO2 decreases, as seen in the 0.125x, 0.25x, and 0.5xCO2 experiments.

A particular feature worth noting is a kink in the 4xCO2 experiment, linked to a shutdown of the Atlantic Meridional Overturning Circulation (AMOC) (Mitevski et al. 2021). Previous research indicates that many CMIP5 and CMIP6 models exhibit substantial AMOC weakening under increasing CO2 forcing (Rugenstein et al. 2013, Winton et al. 2013, Palter 2015, Trossman et al. 2016, Caesar et al. 2020). The reduction in Arctic sea ice can also influence the strength of AMOC by increasing freshwater flux, but this relationship is not unidirectional (Oudar et al. 2017, Sévellec et al. 2017). Mitevski et al. (2021) demonstrated that, in abrupt CO2 experiments using CESM1 and GISS-E2.1-G, the AMOC collapses at 4xCO2 and 3xCO2 respectively, and does not recover under even stronger forcing. Their findings suggest that ocean dynamics play a key role, beyond simple ocean-atmosphere interactions.

Focusing on AAF, a central focus of this study, all three cold AAF values exceed all corresponding warm AAF values (Figure 2d). We also observe that with increasing CO2 forcing intensity (except for the 4xCO2 case), the warm AAF tends to decrease, a trend documented in previous studies and primarily attributed to the relatively small reduction in SIE and the subsequent weaker heat flux exchange between the ocean and atmosphere

doi:10.6342/NTU202404648

under near-ice-free conditions (Deser et al. 2010, Screen & Simmonds 2010, Chung et al. 2021, Liang et al. 2022a). In contrast, differing from the warm AAF (except for the 4xCO2 case), the highest cold AAF occurs in the 0.25xCO2 experiment rather than in the 0.125xCO2 experiment. We explain this by noting that under near-complete ice coverage, sea ice cannot expand significantly further as CO2 is reduced, meaning the incremental SIE increase from 0.125x to 0.25xCO2 is smaller than that from 0.25x to 0.5xCO2 (Figure 2b). Consequently, changes in turbulent heat flux and Arctic SAT are relatively small, resulting in a lower AAF at 0.125xCO2 than at 0.25xCO2. Additionally, the collapse of the AMOC indeed affects the strength of the AAF, as clearly shown in Figure 2d. Despite the collapse of the AMOC, Arctic-related feedbacks continue to produce AA due to the persistent CO2 radiative forcing on the climate system.

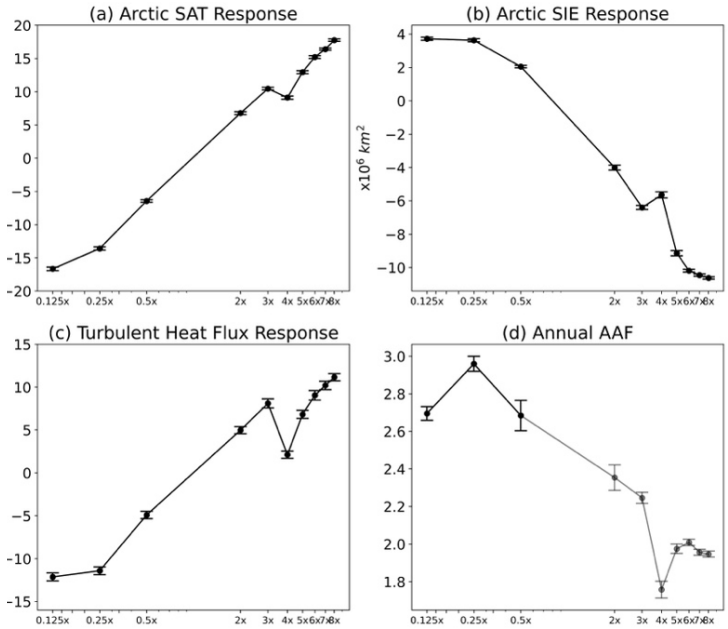

Figure 2: Annual-mean responses during the final 30 simulation years for each nxCO2 experiment: (a) Arctic SAT, (b) Arctic SIE, (c) turbulent heat flux (latent + sensible), and (d) AAF. Error bars represent the 95% confidence intervals, derived using Student's t-distribution.

doi:10.6342/NTU202404648

Here, we conducted feedback analysis to seek a clear explanation for why cold AAF is greater than warm AAF. For each feedback, ERF, and meridional heat transport, we compared their values in the Arctic region with those in the tropical region, following previous studies (Pithan & Mauritsen 2014, Hahn et al. 2021, Beer & Eisenman 2022, Liang et al. 2022b). Figure 3a and b display the results from the 0.125xCO2 and 8xCO2 experiments, comparing their differences and similarities. The Planck, lapse-rate, and albedo feedbacks stand out as the main drivers of both cold and warm AA, as their responses exceed the one-to-one line (gray dashed line), indicating stronger Arctic responses than the global mean. In contrast, water vapor feedback works to reduce AA, and the other feedbacks, along with meridional heat transport, show minimal influence, clustering near the one-to-one line.

Examining these three key feedbacks further; their relative importance differs under increasing versus decreasing CO2. As shown in Figure 3a, for the 0.125xCO2 scenario, the Planck and lapse-rate feedbacks play more prominent roles than the albedo feedback. In the 8xCO2 scenario, all three feedbacks are similarly important. We quantify their relative importance using the Euclidean distance from the one-to-one line (Figure 3c). Under cooling conditions, the Planck and lapse-rate feedbacks clearly surpass the albedo feedback in strength, as indicated by their statistically distinguishable distances. When forcing intensifies (except for the unique 4xCO2 case), the differences in their relative strengths diminish. Under warming conditions, though the albedo feedback becomes more significant, it does not statistically outpace the other two feedbacks, suggesting that all three contribute comparably. These results indicate that the dominance of Planck and lapse-rate feedbacks in cooling scenarios primarily explains the larger magnitude of AA, while the albedo feedback remains essential for maintaining a positive AA signal.

doi:10.6342/NTU202404648

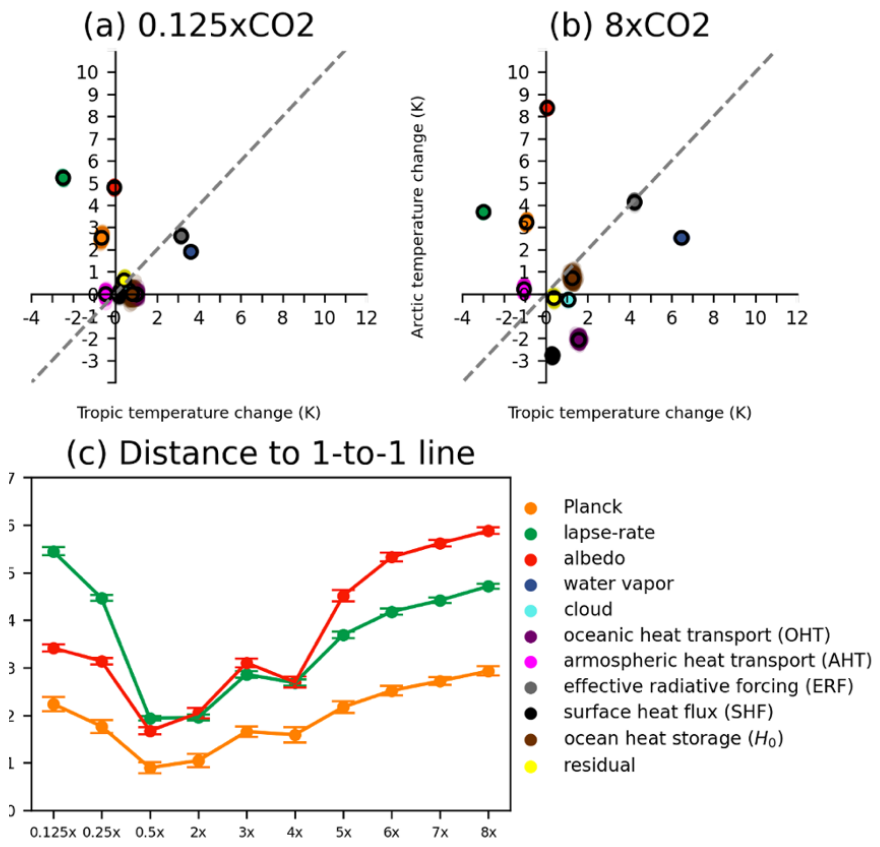

Figure 3: Feedback and meridional heat transport contributions to annual-mean Arctic SAT relative to the tropics under (a) 0.125xCO2 and (b) 8xCO2 abrupt forcings, calculated with radiative kernels. The gray dashed line indicates a one-to-one relationship, helping to identify which mechanisms enhance or reduce AA. In (c), the Euclidean distance of the Planck, lapse-rate, and albedo feedbacks from this line reflects their relative importance. We used 10,000 bootstrap iterations to estimate uncertainties in (a) and (b), while error bars in (c) show 95% confidence intervals from Student's t-distribution.

Finally, we analyze the spatial distribution of the Planck feedback parameter (Figure 4). In warming experiments, the strongest values appear between 85°N and 90°N and diminish somewhat as CO2 increases; in cooling experiments, peak values shift to around 70°N–80°N. This spatial pattern may be linked to changes in sea ice extent. In contrast,

doi:10.6342/NTU202404648

tropical regions show less variation in the spatial scale or intensity of the Planck feedback (Figure 4a). These findings suggest that the enhancement of the Planck feedback in cooling scenarios is driven not only by its overall magnitude but also by its distinct spatial configuration at high latitudes.

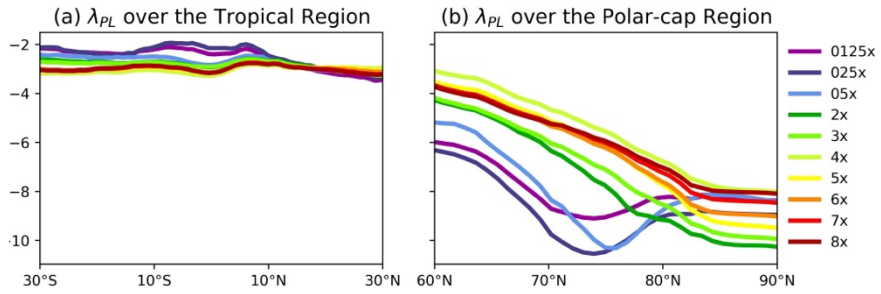

Figure 4: Meridional distribution of the Planck feedback parameter over the (a) tropics and (b) Arctic.

Finally, we analyze the influence of sea ice on the distribution and intensity variations of albedo feedback. This relationship is closely linked to the seasonal retreat of Arctic sea ice during the summer period, when surface albedo feedback from shortwave radiation reaches its maximum. Additionally, it affects the winter boundary layer, where longwave lapse-rate feedback attains its peak (Zhou et al., 2023). This relationship can be explained by the seasonal interactions among the atmosphere, ocean, and cryosphere. Models with greater summer sea ice concentration reduction also show larger reductions in late autumn/early winter sea ice concentration. The more significant reduction in sea ice concentration in autumn and winter is associated with a greater increase in surface sensible and latent heat fluxes among models, along with a greater reduction in temperature inversion. This, in turn, necessitates a stronger correction in the lower-layer lapse-rate feedback, leading to further warming. Across the Arctic, models with greater

doi:10.6342/NTU202404648

sea ice loss produce larger temperature inversion weakening and more substantial corrections in lapse-rate feedback. This relationship also shows spatial robustness.

To further explore how the vertical temperature distribution contributes to the significant role of lapse-rate feedback, we examined the vertically averaged temperature profiles over the polar and tropical regions and their sensitivity to the global mean SAT response (Figure 5). It is evident that under cooling scenarios, the Arctic (representative of the vertically uniform component associated with the Planck feedback) shows greater sensitivity at 1000 hPa, with stronger temperature differences and temperature inversion in the lower troposphere. This indicates that the forcing asymmetry of the lapse-rate feedback has contributions from both the upper and lower layers. In contrast, the temperature gradient distribution in the warming experiments (Figure 5d-j) is relatively smoother, and the gradient distributions are similar across different levels of CO2 forcing. This result demonstrates not only the weaker intensity of lapse-rate feedback in the warming experiments but also the limited impact of increased CO2 on lapse-rate feedback.

doi:10.6342/NTU202404648

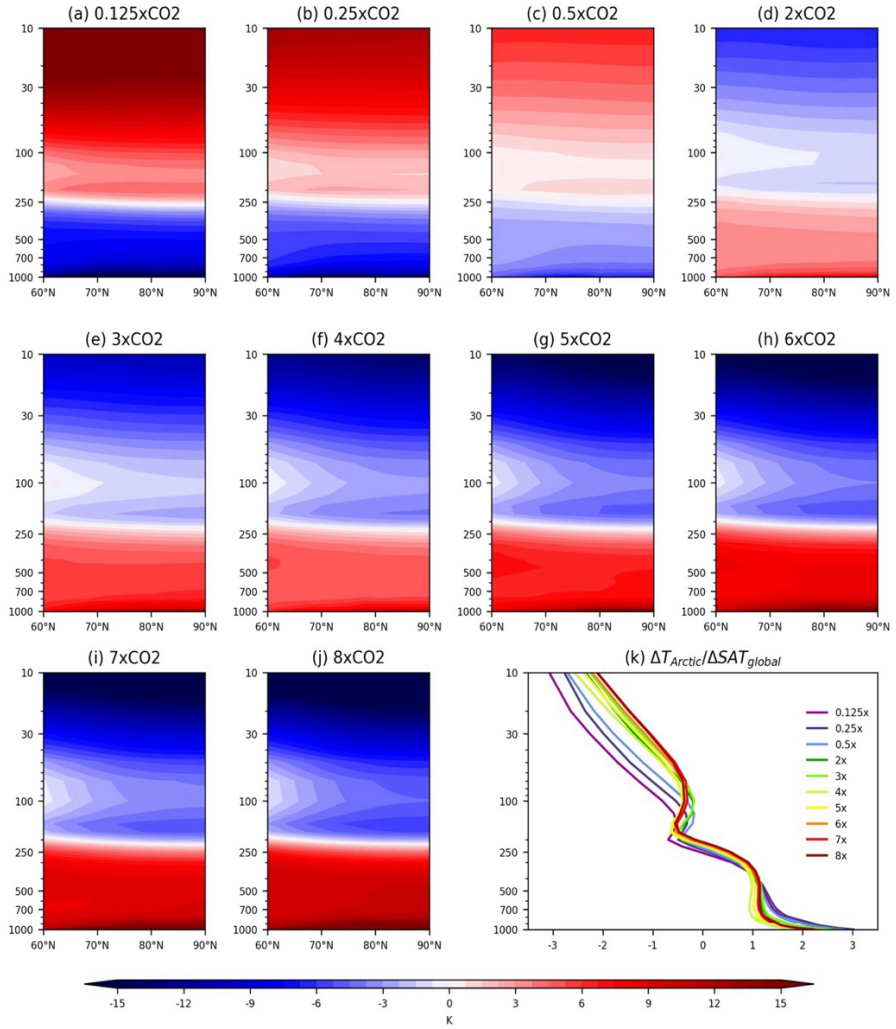

Figure 5: Vertical temperature distribution in the Arctic region. (a-j) Zonal mean for CO2 concentrations ranging from 0.125x to 8x. (k) Changes in the Arctic vertical temperature distribution relative to changes in the global mean temperature.

3.2 Long-term Climate Asymmetry in Warming and Cooling Experiments

Research on surface cooling under greenhouse gas reductions is relatively limited, especially over multi-century timescales. We conducted 1000-year simulations and found

doi:10.6342/NTU202404648

that, after 150 years, global temperatures continue to increase slightly, with the pace of warming remaining nearly constant (Figure 6). In contrast, the average Arctic temperature in the cooling experiments continues to decrease significantly. This indicates that the cooling experiments require a longer time to reach equilibrium compared to the warming experiments. Cold AA remains stronger than warm AA for nearly the entire 1000-year period, though its intensity gradually diminishes over time. At year 150, the surface temperature response in high-latitude regions is similar in magnitude between 2xCO2 warming and 0.5xCO2 cooling (Figure 6b), with the response being slightly larger for 0.5xCO2 than for 2xCO2. After 150 years, the 0.5xCO2 cooling continues and intensifies globally, particularly in high-latitude regions. In contrast, the global and high-latitude warming under 2xCO2 remains relatively stable after 150 years.

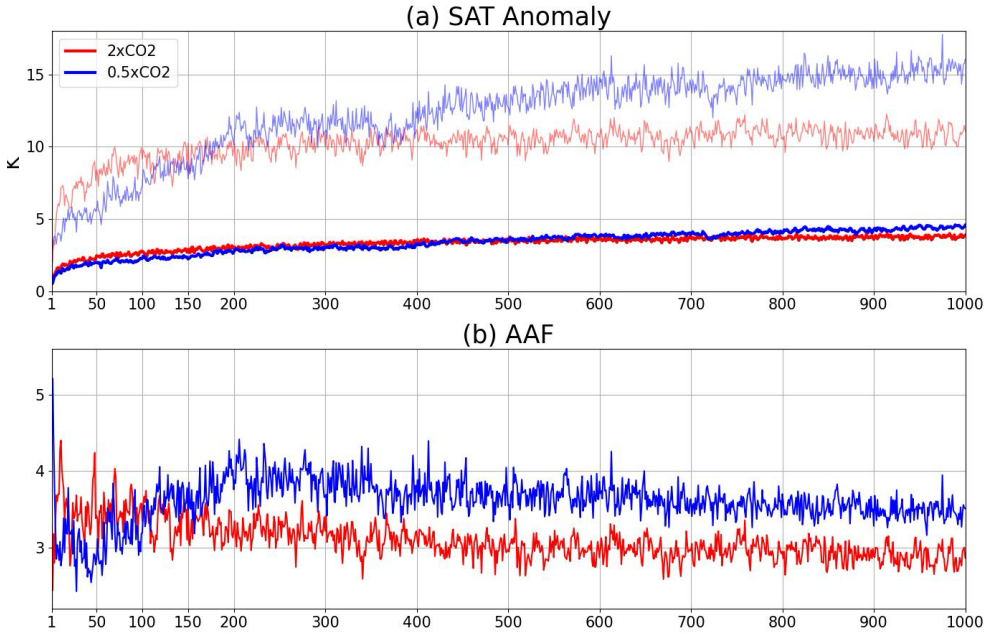

Figure 6: Time series of (a) average SAT anomalies and (b) AAF for the Arctic and global regions over 1000 years.

doi:10.6342/NTU202404648

We used feedback analysis to examine changes in the strength of individual feedbacks. The lapse-rate feedback shows the largest difference between 2xCO2 warming and 0.5xCO2 cooling (Figure 7), making it the primary contributor to asymmetry in the 1000-year simulations. This is likely due to the high heat capacity of the ocean (Stouffer et al. 2004). The ocean can absorb excess heat from the atmosphere and store it over long timescales. This heat storage capacity results in a slower response of the ocean to changes in radiative forcing, leading to a prolonged effect on radiative equilibrium. The results highlight the importance of ocean heat transport for climate equilibrium and its influence on lapse-rate feedback. Lapse-rate feedback is identified as the most significant source of cold AA over both century and multi-century timescales. Additionally, Kay et al. (2024) found that the asymmetry in response is most pronounced at the sea ice edge. Under greenhouse cooling, the sea ice edge gradually shifts southward into midlatitude oceans, a process amplified by positive lapse-rate and surface albedo feedbacks. However, the time evolution of the albedo feedback does not exhibit as large a change as the lapse-rate feedback.

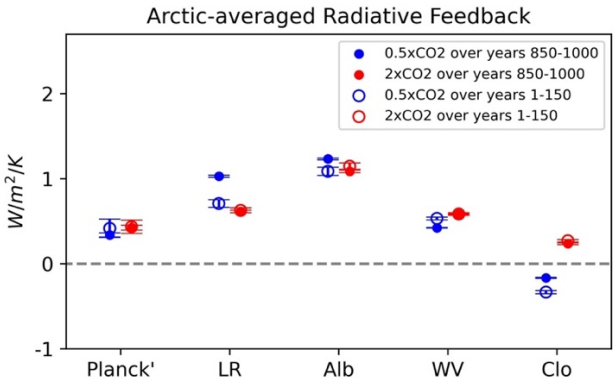

Figure 7: Radiative feedback parameters for the region north of 45°N, showing the first (open circles) and last (solid circles) 150 years of the 2xCO2 (red) and 0.5xCO2 (blue) experiments. Error bars indicate standard deviations across the 150-year averages.

doi:10.6342/NTU202404648

3.3 Asymmetric Interaction and AHT Contributions

We compared the results of feedback locking (Figure 8) with those from the traditional feedback analysis (Figure 3). The results reveal significant differences between these two methods, especially regarding water vapor and lapse-rate feedbacks. In the traditional feedback analysis, water vapor feedback is the largest opposing factor to Arctic amplification. The water vapor feedback parameter is positive everywhere, but its values are much larger in tropical regions than in the Arctic. In contrast, in the feedback locking analysis, water vapor feedback becomes the largest contributor to Arctic amplification. For the lapse-rate feedback, it is the primary contributor to Arctic amplification in the traditional feedback analysis. However, in the feedback locking analysis, its contribution to Arctic temperatures in the cooling experiments diminishes, and it has a near-neutral effect in the warming experiments, as it cools the tropics and Arctic by similar amounts. Lapse-rate feedback no longer plays a dominant positive role in AA within the feedback locking analysis. These differences highlight the importance of interactions between each feedback process and other feedbacks, as well as AHT.

doi:10.6342/NTU202404648

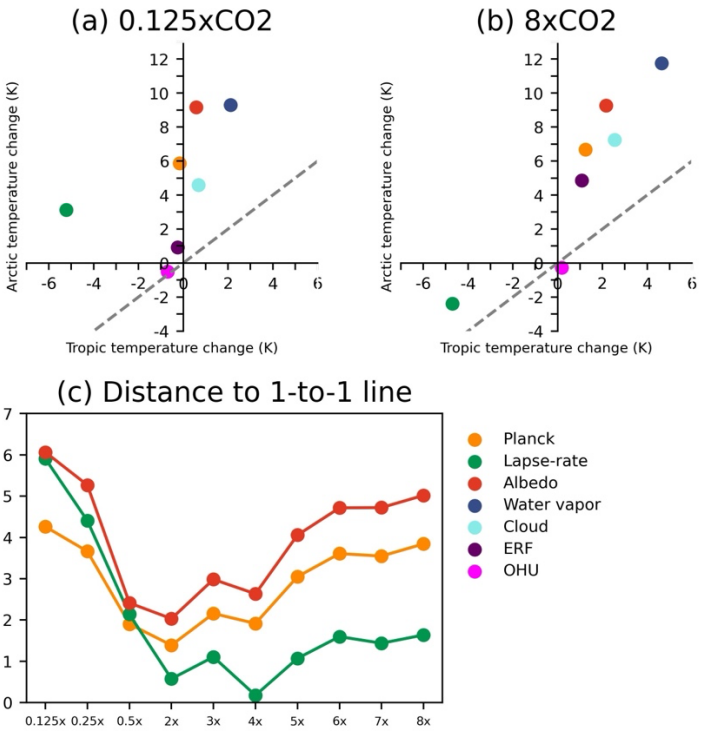

Figure 8: Contributions of individual feedbacks and meridional heat transport to the annual-mean Arctic SAT relative to the tropics under (a) 0.125xCO2 and (b) 8xCO2 forcings, derived through feedback locking analysis. The gray dashed line (one-to-one line) helps distinguish which mechanisms enhance or reduce AA. (c) The Euclidean distance of the Planck, lapse-rate, and albedo feedbacks from the one-to-one line, indicating their relative importance.

In the experiments where water vapor feedback is locked, the MEBM allows the climate system to adjust to the absence of water vapor feedback, leading to changes in temperature. The removal of water vapor feedback reduces warming concentrated in tropical regions, decreasing the temperature gradient between the equator and poles, which in turn reduces AHT in the MEBM or leads to compensatory contributions from other feedbacks (Figure 9b). When water vapor feedback is suppressed, AHT heating slightly increases in the Arctic, while heat is transported away from the equator, causing

doi:10.6342/NTU202404648

tropical cooling. The contribution of feedback interactions increases significantly, indicating that water vapor feedback plays a positive role in supporting other feedbacks. In contrast, the individual contribution of water vapor feedback to the overall feedback experienced in the Arctic is smaller than in the tropics. Overall, water vapor can interact with other positive feedbacks as a positive feedback in the Arctic.

Another feedback that differs significantly between the traditional feedback analysis using radiative kernels and the feedback locking method is lapse-rate feedback, which is also a key mechanism contributing to the asymmetry of Arctic warming (Figure 9a). The direct effect of lapse-rate feedback (individual contribution) reduces the temperature gradient between the equator and poles, leading to a decrease in the meridional temperature gradient, which causes a negative contribution of MSE transport out of the Arctic. Thus, the changes in AHT reduce the extent of Arctic amplification, counteracting the effects of regional feedbacks. Notably, the role of feedback interactions is opposite between the cooling and warming scenarios. Feedback interaction represents the difference between the total equilibrium temperature in the MEBM and the AHT contribution, as compared to the individual contribution. To fully understand the asymmetry, it is necessary to further separate the contributions of upper and lower layers when locking lapse-rate feedback. This helps to identify whether the asymmetry arises from AHT or surface sea ice effects. Overall, we find that in the feedback locking method, lapse-rate feedback leads to tropical cooling, with warming in the Arctic under cooling scenarios and cooling under warming scenarios, providing a more detailed understanding of the asymmetry compared to the traditional feedback analysis.

Other radiative feedbacks show less pronounced differences between the traditional feedback analysis and the feedback locking analysis. The differences may be less noticeable because the positive individual contributions of albedo and Planck feedbacks

doi:10.6342/NTU202404648

lead to a negative AHT contribution and positive effects on other feedbacks, canceling each other out. As a result, their contribution to Arctic warming is greater than their contribution to tropical warming, even when interactions with other feedbacks and AHT are included. For cloud feedbacks, the interactions are stronger in the Arctic compared to the tropics. Mauritsen et al. (2013) emphasized the importance of the coupling between cloud feedbacks, atmospheric circulation, water vapor, and lapse-rate feedbacks in influencing climate change in a deepening troposphere. Climate models may also underestimate the amount of supercooled liquid water in high-latitude clouds, which could lead to an underestimation of the potential contribution of cloud feedbacks to Arctic warming (Middlemas et al. 2020).

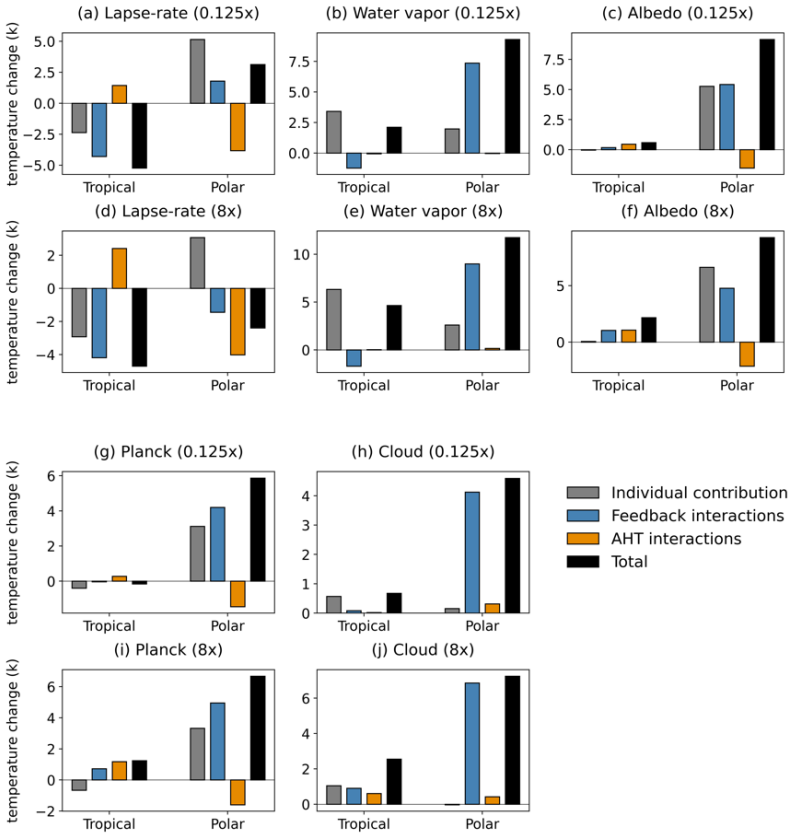

Figure 9: Decomposition of feedback contributions when selectively locking (a) lapse-rate feedback, (b) water vapor feedback, (c) albedo feedback, (d) Planck feedback, and

doi:10.6342/NTU202404648

(e) cloud feedback in the 0.125x and 8xCO2 experiments. These results highlight how constraining individual feedbacks alters the overall AA response under different CO2 forcing scenarios.

Figure 10 shows the spatial comparison between the upper and lower lapse-rate feedback parameters and the sea ice changes in the form of maps. The results indicate that both the upper and lower lapse-rate feedback parameters have a spatial distribution similar to that of sea ice changes. In the cooling experiments, strong signals are concentrated in the Bering Sea, North Pacific, and North Atlantic, while in the warming experiments, the signals are mainly concentrated in the central Arctic Ocean. Sea ice retreat alters the atmospheric temperature structure, particularly after summer sea ice melts, as the warming of the ocean mixed layer weakens the temperature inversion through ocean-atmosphere heat exchange in autumn and winter, which in turn leads to a positive lapse-rate feedback and stronger surface warming. This suggests that sea ice distribution directly influences both the upper and lower lapse-rate feedbacks. We believe that these results highlight the importance of sea ice and surface heat flux in affecting surface temperatures, as well as the limitations of the Radiative Kernels method. In the Radiative Kernels method, lapse-rate feedback is calculated based on the temperature difference between the entire atmospheric column and the surface temperature. Due to weaker vertical convection in the Arctic, the stronger signal is primarily driven by surface temperature. When the surface temperature undergoes significant changes due to sea ice variation, the entire column exhibits a strong lapse-rate feedback signal. This is also related to the stronger stratospheric warming observed in the cooling experiments (Figure 5).

doi:10.6342/NTU202404648

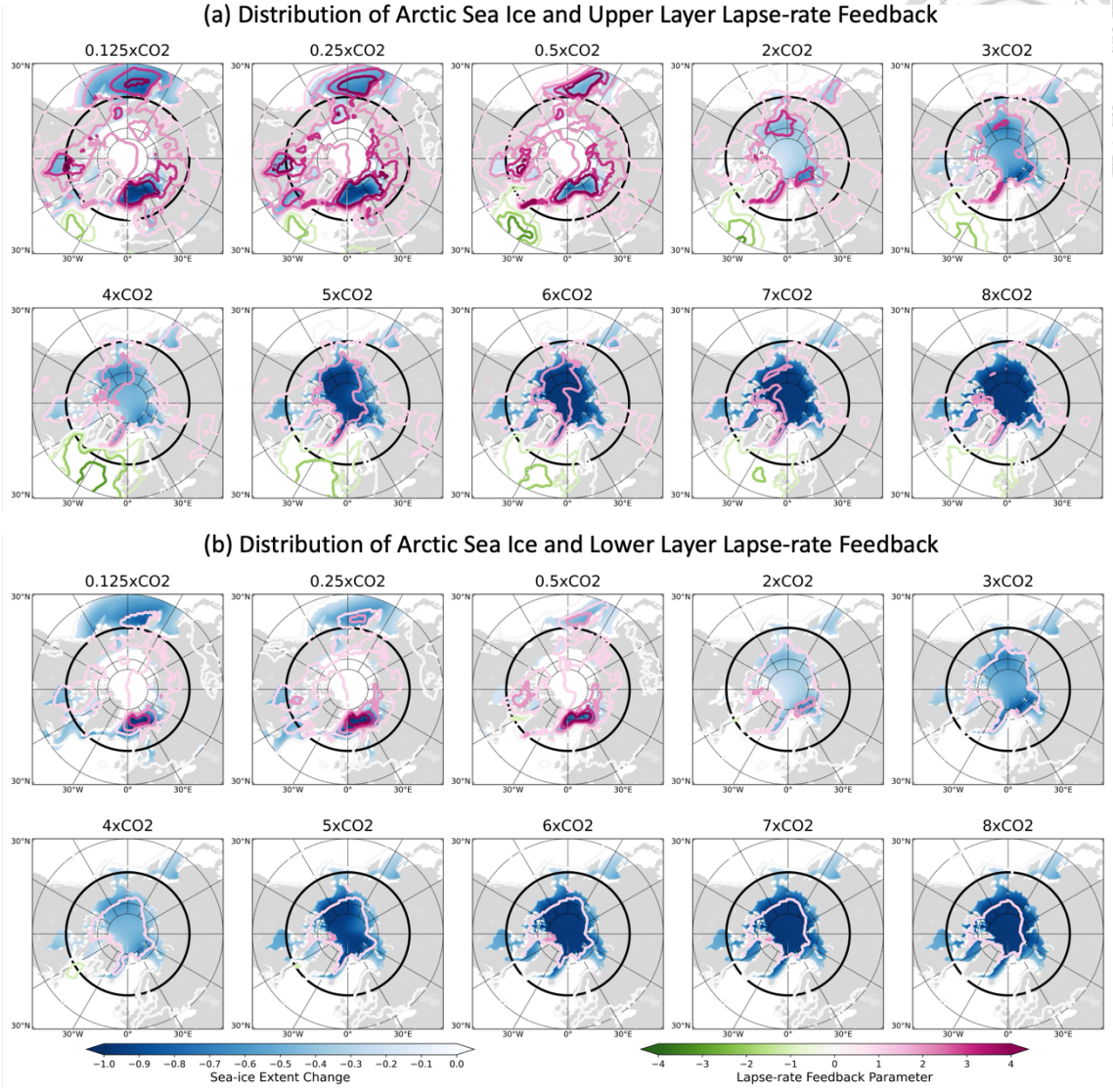

Figure 10: Changes in Arctic sea ice distribution and the distribution of the (a) upper and (b) lower lapse-rate feedback parameters.

We further conducted feedback locking analysis for the upper and lower lapse-rate feedbacks separately to explore how each is influenced by atmospheric heat transport and sea ice distribution. Figure 11 shows that both the upper and lower lapse-rate feedbacks exhibit asymmetry in Arctic amplification, with a larger contribution in the cooling experiments compared to the warming experiments. In the lower lapse-rate feedback

doi:10.6342/NTU202404648

locked experiments (Figure 11a), the temperature changes under the cooling and warming scenarios show similar patterns. The lower lapse-rate feedback is one of the key contributors to Arctic amplification, mainly driven by feedback interactions. Its importance may be much greater than the individual contribution from the lapse-rate feedback alone. In conclusion, the results of the lower lapse-rate feedback demonstrate the positive contribution of the Arctic bottom-warm structure to Arctic amplification. The feedback locking method emphasizes the significant impact of feedback interactions, showing that the lower lapse-rate feedback is a positive contributor to Arctic amplification in both the traditional feedback analysis and the feedback locking method.

In addition to the regional effects of sea ice changes on the atmospheric heat structure at lower atmospheric levels, AHT in the atmosphere also exerts a remote influence on the lapse-rate feedback. Figure 11b shows that the upper lapse-rate feedback induces stronger asymmetry, and it is also the primary driver of changes in AHT interactions. It is worth noting that the upper lapse-rate feedback shows a negative contribution in the warming experiments, whereas it generally has a positive contribution to other feedbacks in the Arctic. This could be due to the top-warm structure of the tropical upper lapse-rate feedback, which enhances the transfer of AHT from the Arctic to the tropics. We suggest that the simplified process of fixing sea ice in the MEBM highlights the influence of lapse-rate feedback on AHT.

doi:10.6342/NTU202404648

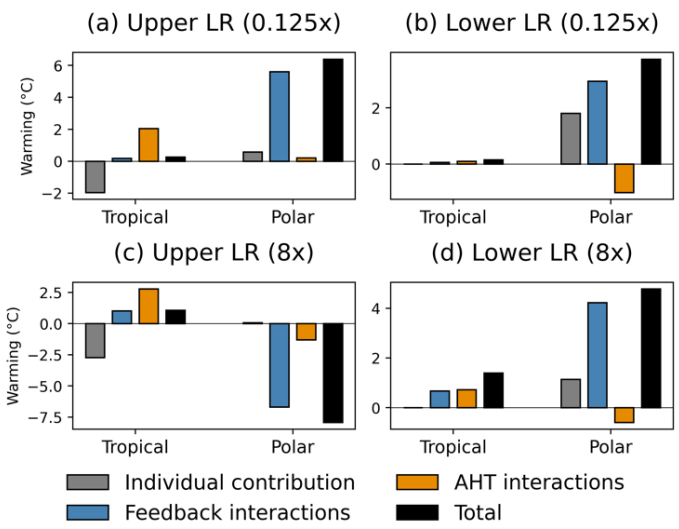

Figure 11: Decomposition of contributions in experiments where the lower lapse-rate feedback (a) and upper lapse-rate feedback (b) are locked under the 0.125x scenario, and where these feedbacks are similarly locked under the 8xCO2 scenario (c-d). These comparisons highlight how variations in the vertical temperature structure influence the magnitude of Arctic Amplification across different forcing scenarios.

Our focus is on the warming experiments, where the regionally averaged upper lapse-rate feedback over the Arctic exhibits a negative value. This differs from results using the radiative kernel method (Figure 12c and d), where the upper lapse-rate remains lower than the lower lapse-rate consistently across latitudes. The negative upper lapse-rate values in the tropics strongly influence meridional energy transport, sending more energy toward lower latitudes and thus affecting the global energy balance and equilibrium temperature.

When comparing cooling and warming experiments, we find that Arctic temperature is influenced by both atmospheric heat transport and sea ice conditions. In the cooling scenarios, the latitude bands where upper lapse-rate feedback remains positive roughly correspond to regions with persistent sea ice coverage, generally north of about 70°N.

doi:10.6342/NTU202404648

Here, upper lapse-rate feedback is stably positive with little spatial variation. Moving south into regions where sea ice seasonally grows or melts, the upper lapse-rate feedback weakens and turns negative. Similarly, in the warming experiments, large reductions in sea ice cause upper lapse-rate feedback to decrease rapidly, leading to an almost complete absence of positive upper lapse-rate feedback signals as the Arctic becomes increasingly ice-free.

During the warming experiments, sea ice loss shifts the ice boundary northward, exposing more open ocean and reducing other feedback contributions, such as albedo feedback. As a result, positive lapse-rate feedback regions shift poleward and diminish in extent, resulting in a net negative lapse-rate feedback contribution in the Arctic. In summary, lapse-rate feedback emerges as the primary mechanism contributing to the asymmetry of Arctic Amplification, interacting with other feedbacks and atmospheric heat transport. This asymmetry stems from the stark differences in sea ice conditions under different CO2 forcing scenarios; the stronger and more positive lapse-rate feedback signature in cooling experiments contrasts with the negative upper lapse-rate feedback in warming experiments shaped by ice-free conditions.

doi:10.6342/NTU202404648

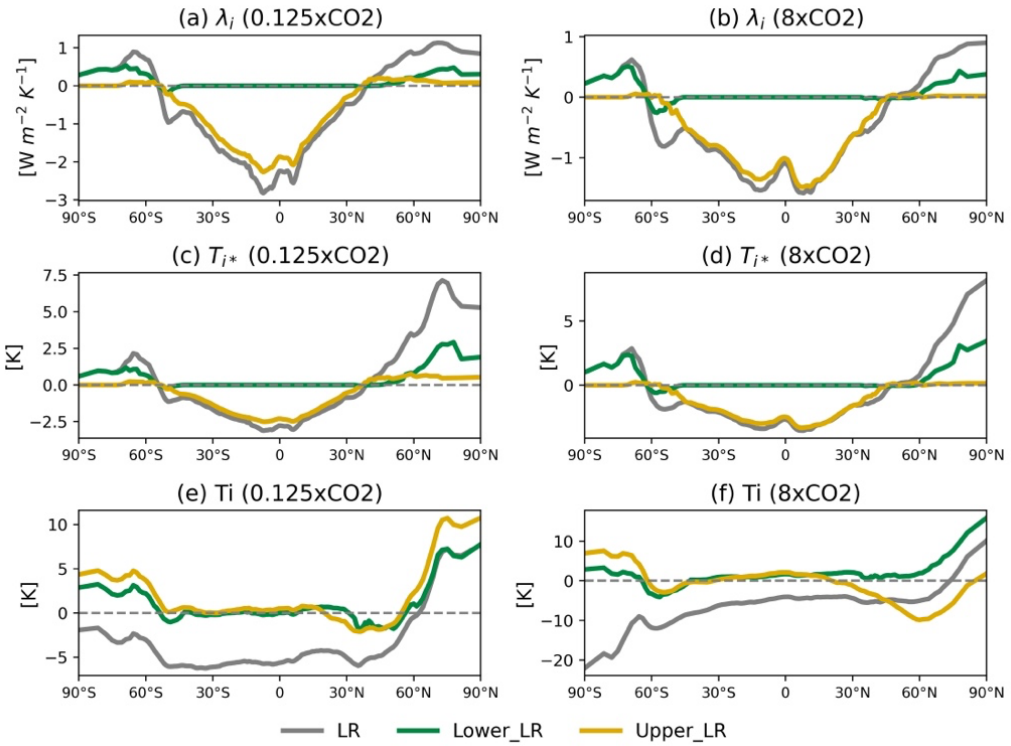

Figure 12: Meridional distribution of (a) feedback parameter, (b) individual temperature contributions (calculated using radiative kernels), and (c) temperature contributions from feedback locking results for the entire column, lower, and upper lapse-rate feedbacks.

Finally, Figure 13 summarizes the distribution of AA strength across all CO2 increase and reduction experiments. In the MEBM, the AA strength for the all-feedbacks-active scenario is generally weaker than that of the GCM, though it still shows the asymmetry where the AA values in the three cooling experiments are generally greater than those in the seven warming experiments. When feedback locking is used to successively deactivate each feedback or surface heat flux, the most pronounced asymmetry is found in the lapse-rate feedback, especially in the upper lapse-rate feedback. The contribution of lower lapse-rate feedback to AA remains relatively consistent across different CO2 forcing levels. Albedo feedback is also an important contributor to AA,

doi:10.6342/NTU202404648

though its asymmetry is less pronounced. The other feedbacks exhibit more uniform contributions overall.

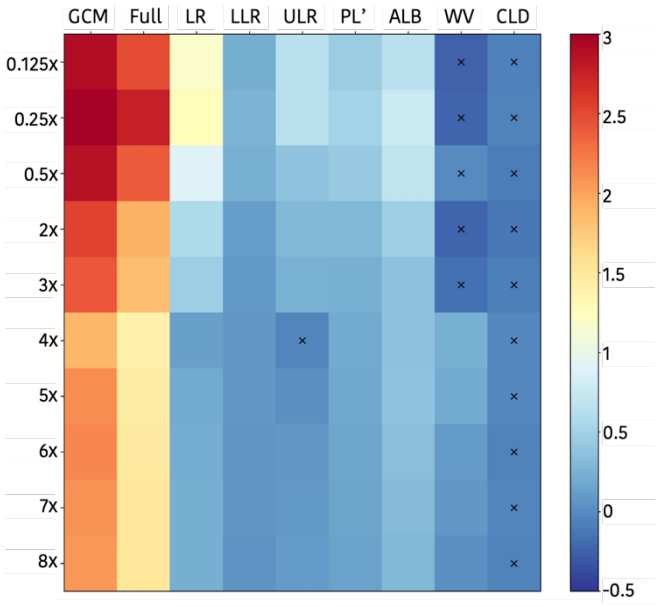

Figure 13: AAF for the GCM with all feedbacks active (full column) and scenarios where each individual feedback is active under CO2 forcing ranging from 0.125x to 8x. Crosses (×) indicate negative values, where the AAF decreases.

doi:10.6342/NTU202404648

Chapter 4 Discussion

We adopted the radiative kernel technique (Soden et al. 2008) to quantify the role of radiative feedbacks in contributing to cold and warm AA. However, the radiative kernel technique may be limited by state dependence. For example, a study using the MPIESM-LR radiative kernel showed that the strength of albedo feedback weakened by 50% in the 4xCO2 experiment compared to the control pre-industrial run (Block & Mauritsen 2013), indicating a significant state dependence of albedo feedback. Indeed, we observed that albedo feedback became less important under 2xCO2 and 0.5xCO2. Jonko et al. (2013) further used the radiative kernel technique to decompose the contributions of each feedback into changes in radiative fluxes and the influence of climate response on temperature changes, finding that variations in Planck and water vapor feedback were primarily driven by changes in radiative fluxes associated with shifts in climate states. We also noted a slight increase in the residuals averaged over the Arctic when CO2 concentrations exceed five times the pre-industrial levels, reflecting larger changes in the polar mean when using the radiative kernel technique, as shown in Jonko et al. (2013). Therefore, further research is needed to validate the application of the radiative kernel technique in both warming and cooling states.

According to Jansen (2017), changes in atmospheric CO2 concentrations significantly alter ocean circulation and stratification, thereby affecting the uptake and release of carbon by the oceans. However, these changes are not entirely symmetrical across different ocean regions. When CO2 increases, global warming shrink sea ice extent, weakening deep ocean stratification, particularly in the deep waters around Antarctica, making it easier for oceanic carbon to be released back into the atmosphere. In contrast,

doi:10.6342/NTU202404648

when CO2 decreases, lower temperatures encourage sea ice growth and brine rejection, strengthening deep ocean stratification, which limits the release of carbon from the deep ocean. This asymmetry in ocean carbon dynamics implies that different ocean regions respond to CO2 changes in varying degrees of carbon uptake and release, potentially influencing long-term global carbon cycles and climate trends. Additionally, shifts in ocean heat distribution patterns also affect long-term climate. Fabiano et al. (2024) showed that the rate of warming in the Southern Ocean significantly increases over long timescales, with heating primarily concentrated in the South Atlantic and Indian Oceans under lower forcing scenarios, and expanding to the Pacific under higher forcing scenarios. This aligns with the findings of Rugenstein et al. (2016), who noted that heat uptake efficiency in the Southern Ocean is lower under higher forcing scenarios, leading to shifts in ocean heat distribution across different timescales. Consequently, the interpretation of long-term changes in lapse-rate feedbacks in this study must consider regional variations in ocean energy distribution to confirm the drivers of feedback mechanism changes over century timescales.

We employed the classic separation of lapse-rate and water vapor feedbacks, allowing for a more direct comparison with traditional feedback analyses that also adopt this separation. However, it is important that the quantification of feedback contributions depends on how feedbacks and contributions are defined, which should be considered when comparing studies. A recent study by Russotto & Biasutti (2020), which also employed the feedback locking method, investigated how feedbacks contribute to Arctic amplification in a set of idealized slab ocean aquaplanet GCM simulations that excluded sea ice. Similar to our findings, they observed a positive contribution of water vapor feedback to Arctic amplification. However, their simulations lacked albedo feedback, which is a major positive feedback in the Arctic and interacts significantly with water

doi:10.6342/NTU202404648

vapor feedback in our results—though quantifying this interaction is challenging. Another point worth noting is that both feedback locking and traditional feedback analysis typically assume a linear relationship between feedbacks and warming, where surface temperature changes are approximately proportional to the feedbacks. Under this assumption, the vertical temperature changes in the atmosphere are generally attributed to lapse-rate feedback. Henry & Merlis (2019) found that when linearizing the Stefan-Boltzmann law, Planck feedback is expected to weaken Arctic amplification due to the nonlinear nature of the law altering the vertical warming structure. Specifically, the enhanced lapse-rate feedback partially diminishes the impact of the weakening Planck feedback, leading to a strong AA.

One limitation of the feedback locking analysis to consider is that the results depend on the degree of simplification in the complex energy exchange processes within the model and on the assumption of state-dependent feedback parameters. In GCMs, these parameters may evolve with changing climate conditions. As such, the temperature changes in the MEBM feedback locking simulations are expected to differ from those in comprehensive GCM feedback locking simulations, where GCMs represent more processes and effectively have feedback parameters calculated interactively. In contrast, in the MEBM simulations presented here, each feedback parameter remains fixed when other feedbacks are locked. Although this is anticipated to be a source of inaccuracy, previous studies have shown that treating feedback patterns as time-invariant provides a relatively accurate approximation for climates ranging from pre-industrial to 2xCO2 conditions (Dai et al. 2020).

doi:10.6342/NTU202404648

Chapter 5 Conclusion

In this study, we utilized a series of abrupt CO2 experiments using a state-of-the-art fully coupled climate model to compare the phenomena and mechanisms behind cold and warm AA. Our findings show that when CO2 concentrations decrease, AA intensifies more than it does under CO2 increases, indicating a pronounced asymmetry. Feedback analysis reveals that enhanced lapse-rate feedbacks plays key role in driving cold AA, which interact with sea ice reduction, turbulent heat flux, and SAT. This asymmetry aligns with the research framework summarized in Figure 14, where both feedback decomposition and feedback locking approaches highlight the importance of lapse-rate feedback and its interplay with atmospheric heat transport and sea ice distribution. While the global surface temperature may respond differently to increases or decreases in CO2, the Arctic demonstrates a distinct set of underlying mechanisms that shape its asymmetric response. Further research is needed to better understand the feedback processes and radiative forcings contributing to Arctic asymmetry, as these may fundamentally depend on the nonlinear dynamics of the Arctic climate response (Sumata et al. 2023).

doi:10.6342/NTU202404648

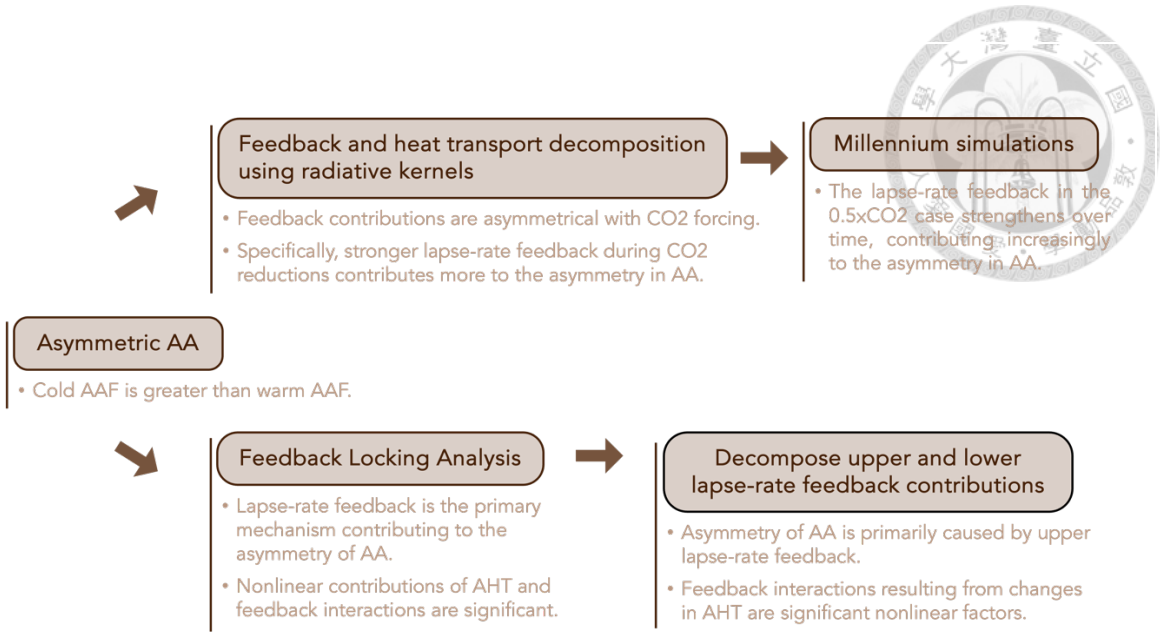

Figure 14: Research framework exploring whether the intensity and mechanisms of AA are symmetric.

In quantifying the physical mechanisms behind high-latitude lapse-rate feedback, we distinguished the effects of local sea ice processes from those of remote atmospheric energy transport, showing a clear spatial link between lapse-rate feedback and sea ice retreat. By analyzing sea ice distribution changes, the connection between positive lapse-rate feedback over the Arctic Ocean and reduced sea ice became clearer, consistent with the feedback and heat transport decomposition highlighted in the framework. Additionally, century-scale coupled simulations demonstrate that the response timescales differ for warming and cooling scenarios, with surface warming responses occurring on decadal scales, while surface cooling responses emerge over centuries. We also identified lapse-rate feedback as the most significant source of asymmetry, a finding supported by feedback locking analysis that reveals significant and nonlinear interactions between atmospheric heat transport and feedbacks. Furthermore, the ocean's long-term adjustment, influenced by vertical mixing and deep-ocean heat transfer, indirectly affects the climate

doi:10.6342/NTU202404648

system's response timescale.

The weakening of warm AA is primarily attributed to the changing relationship between lapse-rate feedback and other feedbacks, particularly as upper-level lapse-rate feedback transitions from positive to negative under increased CO2. In summary, this study explored the roles of various feedback mechanisms in cold and warm AA through both traditional feedback analysis and feedback locking methods, emphasizing how the interplay between sea ice changes, atmospheric heat transport, and lapse-rate feedback leads to asymmetric Arctic responses. Our results suggest that considering both CO2 increases and decreases offers a richer perspective on AA's underlying mechanisms and can inform climate policy and future carbon management strategies. Moreover, our findings indicate that aerosol-induced cooling could also produce conditions leading to cold AA. While the geographic distribution and temporal evolution of aerosol radiative forcing differ from those of CO2 forcing, previous studies have suggested that the cooling effects induced by aerosol loading could lead to the occurrence of cold AA (Feichter et al. 2004, Ming & Ramaswamy 2009, Jiang et al. 2020, England et al. 2021).

doi:10.6342/NTU202404648

APPENDIX

Global warming is characterized by an increase in SAT, with an accelerated rise particularly evident in the latter half of the 20th century (Eyring et al. 2021). However, changes in SAT can be influenced by various factors. The first source of variability comes from external forcings, such as increases in greenhouse gas concentrations, variations in anthropogenic and natural biomass burning aerosols, ozone depletion, solar fluctuations, volcanic eruptions, and land-use changes. This externally driven variation is referred to as forced variability. The second source of variability arises from internal processes within the atmosphere, oceans, cryosphere, land, and biosphere, along with their interactions (Cassou et al. 2018). This type of variability is known as internal variability, manifesting fluctuations inherent to the climate system that can emerge even without the effect of external forcings.

While forced variability has largely driven the large-scale and long-term trends in SAT over the 1900–2020 period (Deser et al. 2012, Kay et al. 2015), the specific contributions of internal and forced variability remain complex and not fully understood. In particular, internal variability plays a key role on shorter timescales and smaller spatial scales. For instance, the leading mode of internal variability in global SAT is the El Niño Southern Oscillation (ENSO), marked by significant temperature anomalies in the equatorial Pacific and widespread teleconnections, with a periodicity of 2 to 7 years (Wang & Picaut 2004, Wang et al. 2017). Other important modes of internal variability include Interdecadal Pacific Variability (Newman et al. 2016) and Atlantic Multidecadal Variability (Zhang et al. 2019), which influence climate patterns over decadal to multidecadal scales. The slowed warming observed during 2002–2012, often termed the

doi:10.6342/NTU202404648

global warming hiatus, has been linked to Interdecadal Pacific Variability (Kosaka & Xie 2013, Meehl et al. 2013, England et al. 2014) and reduced heat uptake by the Atlantic and Southern oceans (Chen & Tung 2014, 2018). Additionally, internal variability may include centennial to multi-centennial fluctuations, potentially influencing trends observed from 1900 to 2015 (Bonnet et al. 2021, Fan et al. 2023)

Distinguishing between forced and internal variability is crucial in detection and attribution studies, as it enables us to separate the climate response to radiative forcing changes and gain a clearer understanding of internal climate variability. However, instrumental records are available only from 1850 onwards with only one realization, and the relatively short duration of these observations complicates efforts to accurately characterize internal variability. Methods for identifying both types of variability include approaches that consider linear trends (Swart et al. 2015, Vincent et al. 2015), quadratic trends (Enfield & Cid-Serrano 2010), global-mean values (Trenberth & Shea 2006) and a linear regression (Ting et al. 2009) as estimates of forced variability. Nonetheless, these methods may not capture the full temporal evolution of temperature accurately, particularly struggling to account for abrupt cooling events following large volcanic eruptions (Schmidt et al. 2018). To remedy this issue, a family of methods based on linear inverse modeling (Penland & Matrosova 1994, 2006) and empirical orthogonal functions (EOFs, Ting et al. 2009) has been utilized to separate the internal variability modes and investigate its relation to other climate components, such as the Atlantic meridional overturning circulation (e.g., Frankignoul et al. 2017).

An alternative approach to separate internal variability from forced variability is to conduct climate model simulations with large ensemble members, each with different initial conditions (Deser et al. 2020). This methodology has been employed to overcome the limitations of sparse observational data. Previous studies have estimated forced

doi:10.6342/NTU202404648

variability using the ensemble mean, which is assumed to effectively reduce the variance associated with internal variability by a factor equal to the number of ensemble members (Harzallah & Sadourny 1995, Hawkins & Sutton 2009, Ting et al. 2009, Solomon et al. 2011, Deser et al. 2014, Frankcombe et al. 2015). Consequently, many modeling centers have conducted extensive ensemble simulations, often with more than 10 ensemble members (Jeffrey et al. 2013, Rodgers et al. 2015, Deser et al. 2020). Some results of these simulations are archived as single-model initial-condition large ensembles (SMILEs; Deser et al. 2020), providing a valuable dataset for developing methods to distinguish between forced and internal variability. Additionally, using members of a large ensemble as surrogate observations allows for direct comparison of individual results with the ensemble mean.

The Community Earth System Model 2 (CESM2) Single Forcing Large Ensemble Project (https://www.cesm.ucar.edu/working-groups/climate/simulations/cesm2single-forcing-le) was developed to explore the roles of both forced and internal variability. This project includes four sets of simulations, each with more than 10 members, driven by individual climate forcing agents: greenhouse gases (GHG), anthropogenic aerosols (AER), biomass burning aerosols (BMB), and a combination of other factors (EE), including volcanic eruptions, solar irradiance variations, ozone, and landuse changes. Alongside the all-forcing simulations from the CESM2 Large Ensemble Project (https://www.cesm.ucar.edu/community-projects/lens2), this dataset allows for detailed analysis and quantification of the contributions of different forcings to climate change and variability.

Recent studies have been widely attempted to exploit artificial intelligence techniques to study the forced and internal variability using large ensemble simulations (e.g., Bône et al. 2023, Ham et al. 2023). For example, Bône et al. (2024) trained a U-Net

doi:10.6342/NTU202404648

model with CMIP5/6 simulations to filter out the internal variability signal in surface air temperature, leaving forced variability. In contrast, Sweeney et al. (2023), using CMIP6 and CESM2 large ensemble, trained a neural network to single out a unique temperature trend pattern driven by internal variability. These studies motive us to apply similar deep learning approach to large-ensemble simulations. In this study we use the simulation sets of CESM2 single forcing large ensemble to train a convolution neural network to separate the forced variability from internal variability for each single forcing runs.

We begin by examining the annual-mean SAT anomalies and variability from the CESM2 single-forcing large ensemble. Figure 1a shows the mean SAT anomalies from 2020 to 2050 for all-forcing simulations (herein referred to as ALL). Typical global warming spatial patterns emerge, including amplified warming in the Arctic, stronger warming over land compared to oceans, reduced warming in the North Atlantic (also known as the 'Atlantic warming hole'), and El Niño-like warming in the eastern tropical Pacific. The variability, quantified by the standard deviation of SAT anomalies, is highest in the Arctic, particularly in the Barents-Kara Seas (Figure 1b). This is largely due to significant sea-ice retreat and the related sea ice-albedo feedback, which contribute to substantial year-to-year variation. Other regions with notable variability include the North Pacific and the eastern tropical Pacific.

doi:10.6342/NTU202404648

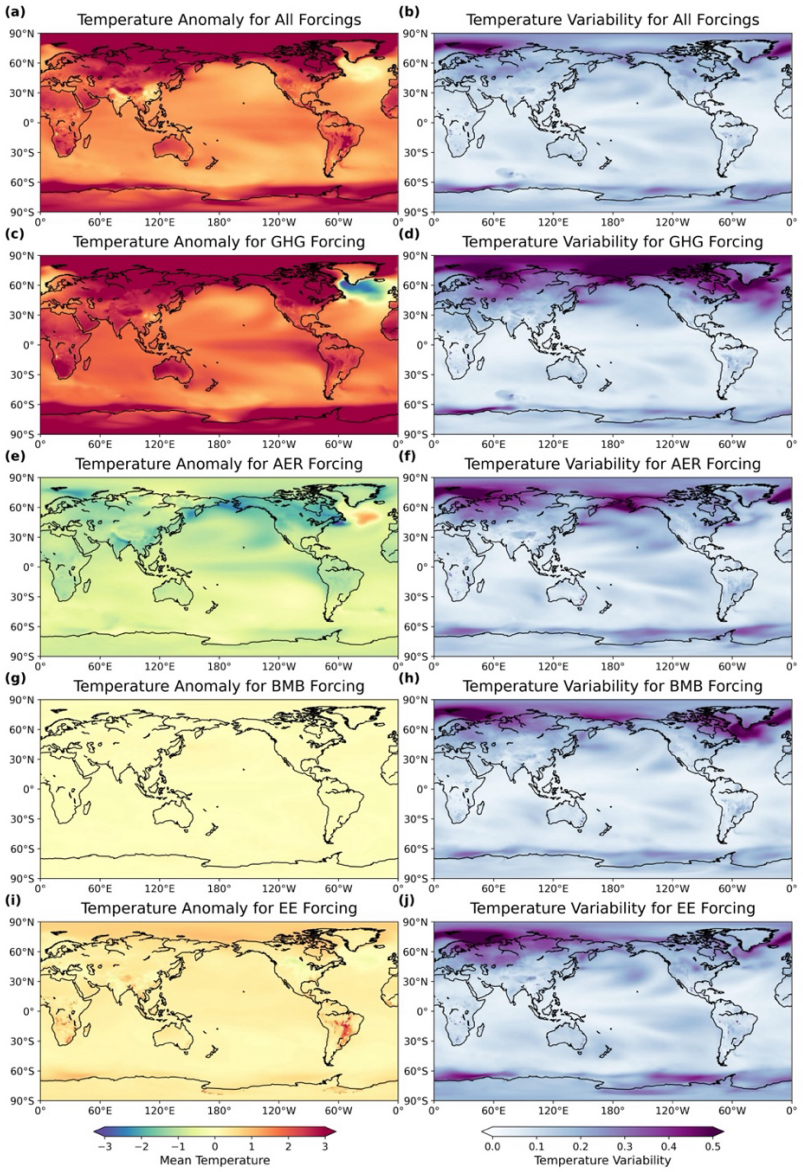

Figure 1: Temperature anomaly and internal variability, defined as the standard deviation across 15 ensemble members, are examined for the period 2020 to 2050 in CESM2. The panels show different forcing scenarios: (a, b) all forcings combined, (c, d) greenhouse gas (GHG) forcing, (e, f) aerosol (AER) forcing, (g, h) biomass burning (BMB) forcing, and (i, j) everything else (EE) forcings.

The GHG simulation exhibits similar mean warming and variability patterns (Figures 1c and d) compared to the ALL simulation, although with an overall greater

doi:10.6342/NTU202404648

magnitude. In contrast, the AER simulation results in global cooling patterns (Figure 1e) that are opposite in sign to the GHG simulation. Notably, regions of strong cooling in the AER simulations do not align precisely with regions of strong warming in the GHG simulation. For example, the largest cooling is not observed in the Arctic, but rather in the North America. While the mean SAT anomalies are smaller in the Arctic, the variability remains high (Figure 1f). The mean SAT anomalies in the BMB and EE simulations are much weaker (Figures 1g and 1i); however, substantial variability persists in the Arctic (Figures 1h and 1j), indicating the amplified effect of the strong sea-ice albedo feedback.

We then examine the time series of global-mean and Arctic-mean SAT anomalies over the 1850–2050 period. The GHG forcing drives global and Arctic warming, beginning in the early 1900s and accelerating after the 1950s (red lines in Figures 2a and 2c). In contrast, the AER forcing induces sustained global and Arctic cooling from the 1950s, leveling off around 2010 (blue lines in Figures 2a and 2c). The other two forcing agents cause comparatively smaller variations in global and Arctic SAT (yellow and green lines in Figures 2a and 2c). In the EE simulation, notable features are still evident, such as the SAT drop in the early 1990s due to the Pinatubo volcanic eruption. The sum of all single-forcing time series closely resembles the ALL simulation (gray lines in Figures 2a and 2c), indicating a high degree of additivity for Arctic and global SAT.

doi:10.6342/NTU202404648

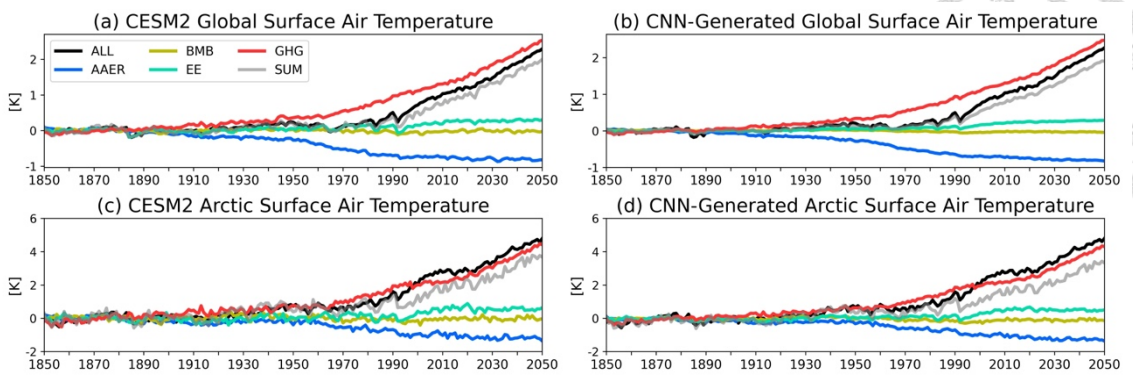

Figure 2: (a) Global and (c) Arctic annual mean surface air temperature anomalies in CESM2, referenced to the 1850–1899 period. The data are processed using the ensemble mean to highlight the forced signal, serving as the target air temperature reference for CNN-based predictions of the forced signal. The CNN-generated forced signal is depicted in (b) global and (d) Arctic annual mean anomalies.

We use a convolutional neural network (CNN) to carry out the training task and present its architecture in Figure 3. The input to the network is a single time step of a global SAT map with a spatial resolution of 96x144. The CNN architecture consists of two sequential combinations of convolutional layers with ReLU activation and max-pooling operations, followed by three fully connected layers. The output layer consists of 10 values, representing the global and Arctic averages for each of the five different forcing types (ALL, AER, BMB, EE, GHG) for the input SAT map at the specified time step. This network architecture effectively captures and transforms spatial patterns in SAT data, enabling the model to predict the corresponding global and Arctic averages under different forcing scenarios.

doi:10.6342/NTU202404648

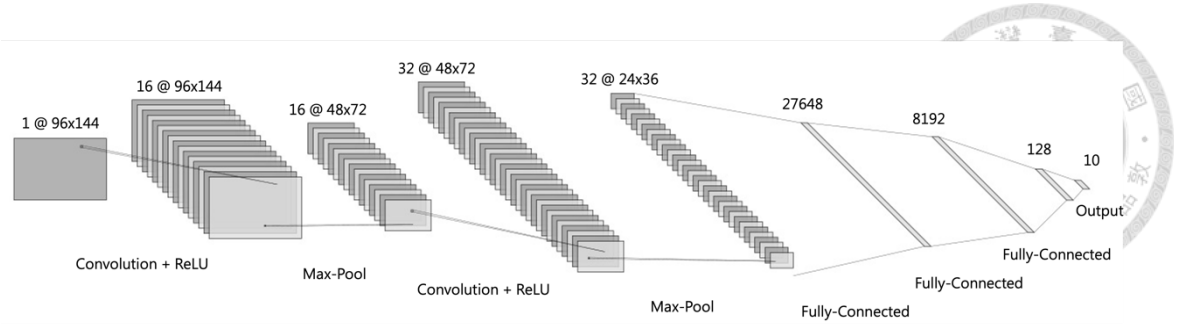

Figure 3: A schematic of the CNN architecture, where the input consists of monthly mean global temperature maps. The architecture includes two convolutional layers and two maximum pooling layers, followed by three fully connected layers that produce 10 output values. These outputs correspond to the global and Arctic mean responses to all, GHG, AER, BMB, and EE forcings, respectively.

The CNN model effectively generates the forced component for each forcing agent using a single member that was not involved in the training process (Figures 2b and 2d). The CNN predictions capture the key characteristics of GHG-induced warming, AER-induced cooling, and the smaller SAT variations associated with BMB and EE. Notably, the CNN-predicted SAT time series also replicate the specific SAT declines in the early 1990s resulting from the Pinatubo volcanic eruption in the ALL and EE simulations. One discrepancy is that the CNN-generated global SAT time series tend to appear smoother than the true forced time series, especially for the EE and BMB simulations, which exhibit weaker variability. However, this discrepancy is less pronounced in the Arctic SAT time series.

doi:10.6342/NTU202404648

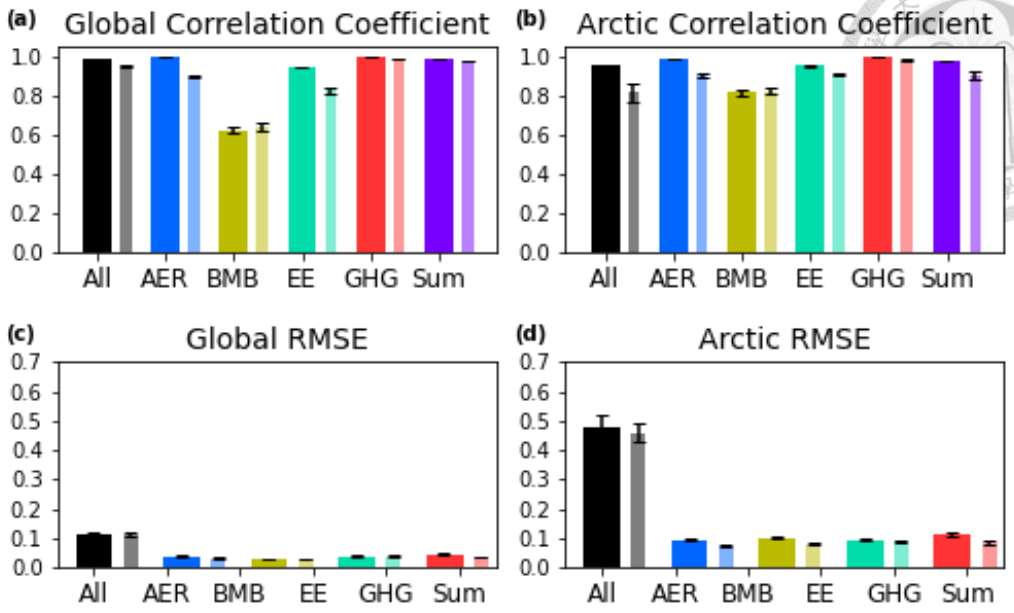

Figure 4: Correlation coefficients between the annual data of the (a) global and (b) Arctic targets from CESM2 and the corresponding CNN-generated results. Panels (c) and (d) show the root-mean-square error (RMSE) for the global and Arctic regions. Error bars represent the standard deviation across 15 ensemble members, with thinner bars indicating the results after detrending.

To further evaluate the CNN's performance, we calculate the temporal correlation coefficient and the RMSE between the CNN-predicted time series and the true time series for the 1850–2050 period. With the exception of the BMB case, the correlation coefficients are relatively high for both global-mean and Arctic-mean SATs (Figures 4a and 4b), indicating that the CNN effectively captures the temporal variability of the forced SAT responses. The lower correlation coefficient for the BMB case may stem from the smoother time series predicted by the CNN, as previously discussed, which significantly reduces the year-to-year variation in SATs associated with BMB forcing. While the correlation coefficient provides insight into how well the CNN model can predict temporal variability, the RMSE highlights potential mean bias between the CNN-

doi:10.6342/NTU202404648

predicted and true time series. We observe that the RMSE for the ALL case, in both global and Arctic time series, is higher than the RMSEs for each individual forcing (Figures 4c and 4d). This finding suggests that although the CNN captures year-to-year variability well for the ALL case, it may mis-estimate the mean state. Due to the amplified Arctic SAT response resulting from Arctic amplification, the RMSE for the Arctic time series is greater than for the global one. To further examine this long-term trend effect, we also remove the linear trend for each case and repeat the correlation coefficient and RMSE calculations, yielding similar results (thin bars in Figure 4).

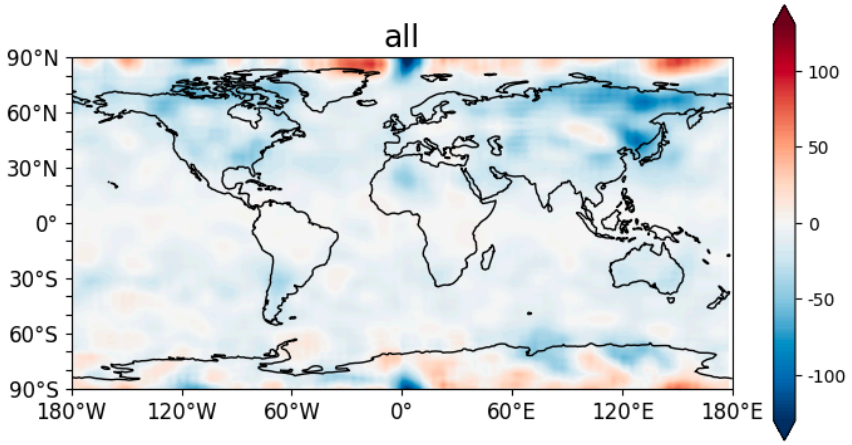

Figure 5: Occlusion sensitivity using CESM2 dataset.

We next aim to improve the interpretability of the CNN by conducting an occlusion analysis (Zeiler 2014, Ham et al. 2023). The heatmap generated from this analysis highlights regions with high values, both positive and negative (Figure 5). A prominent area is the Arctic, where significant values appear in the Arctic Ocean, contributing positively to the CNN's learning across most regions in the northern high-latitudes. This pattern aligns well with the AA phenomenon. However, focusing on the AA hotspot, specifically the Barents-Kara Seas with the highest amplification (Zhong et al. 2018,

doi:10.6342/NTU202404648

Chen et al. 2021, Kumar et al. 2021), we observe that the heatmap values are not exceptionally high in this area. This suggests that the CNN may not fully capture this prominent feature to distinctly separate the forced Arctic and global SAT signals. Notably, a negative value is present across the Fram Strait, which may be linked to the climatological ocean currents and sea-ice transport out of the Arctic domain.

In land areas, regions such as North America and northeastern Siberia and Asia show large negative values. The combination of these negative values and the positive values over the Arctic might reflect the so-called Arctic warm-continental cold SAT pattern associated with AA (e.g., Cohen et al. 2014, Kug et al. 2015) or internal variability (Francis & Skific 2015, Vavrus 2018). Interestingly, values over land are generally larger than those over the oceans, resonating with the dominant global warming spatial feature where land warms more than the ocean (Joshi et al. 2008, Boer 2011, Byrne & O'Gorman 2013). Additionally, large values are observed in Antarctica, with positive values in eastern Antarctica and negative values in western Antarctica. This may represent a zonal wavenumber-1 pattern, possibly related to the variability in large-scale atmospheric circulation in the Southern Hemisphere.

doi:10.6342/NTU202404648

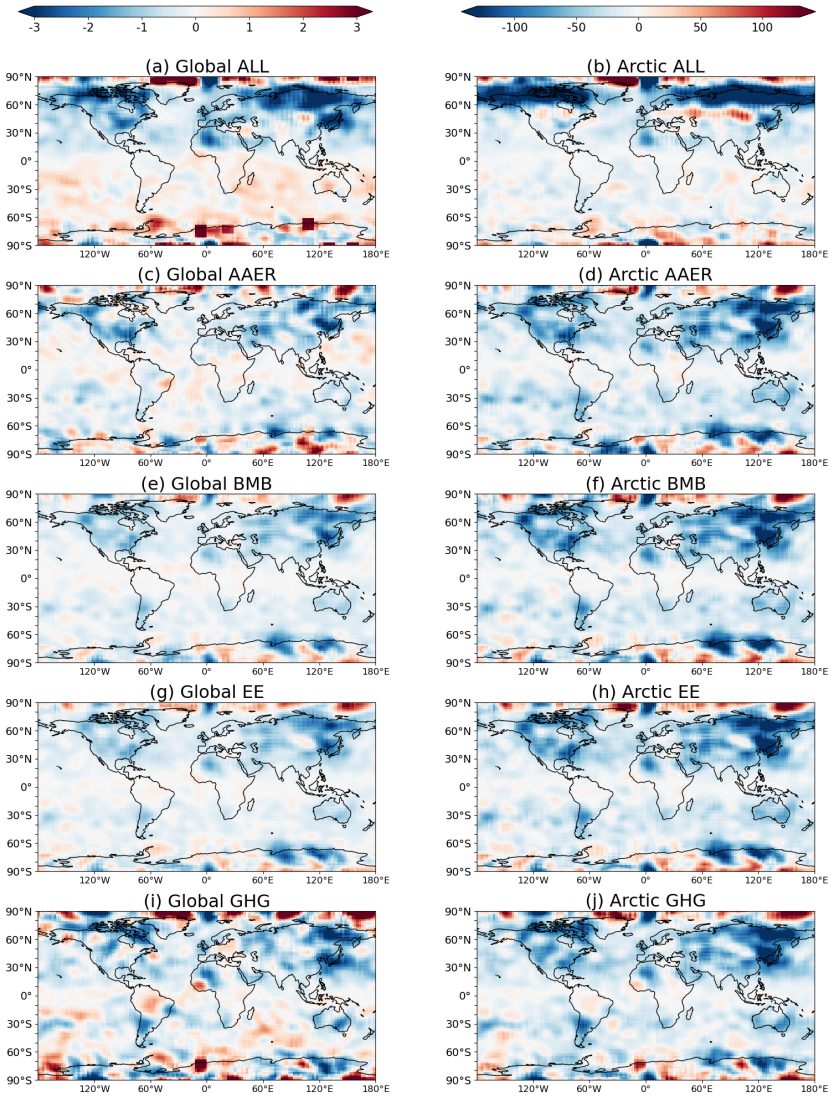

Figure 6: Occlusion sensitivity using CESM2 dataset for (a, b) ALL forcing and single forcing (c, e, g, i) global and (d, f, h, j) Arctic average.

The occlusion analysis also enables us to focus on a single output, allowing us to create heatmaps attributed to one specific forcing agent. For each individual forcing, we observe a spatial distribution similar to that shown in Figure 6. One notable feature that stands out from the ALL heatmap is the overall negative values in the Northern Hemisphere and positive values in the Southern Hemisphere. This pattern reflects the inter-hemispheric gradient, a unique spatial response to global warming that has been

doi:10.6342/NTU202404648

widely discussed in previous studies (Chiang & Friedman 2012, Ma et al. 2012, Vallis et al. 2015). The result suggests that the CNN has learned this feature, aiding in the removal of internal variability and the distinction of forced responses.

The CNN training exercise is based on CESM2 single-forcing simulations with large ensembles. A relevant question that follows is whether this trained CNN can be applied to simulations from other climate models with single forcings. If so, it would suggest that the trained CNN model is generalizable to other simulated datasets. To test this, we use data from the Detection and Attribution Model Intercomparison Project (DAMIP, https://damip.lbl.gov/) under CMIP6. We select four models that provide more than 10 ensemble members for both GHG and AER simulations. It is noted that the four models from DAMIP did not offer BMB and EE simulations. The results are presented in Figures 7 and 8.

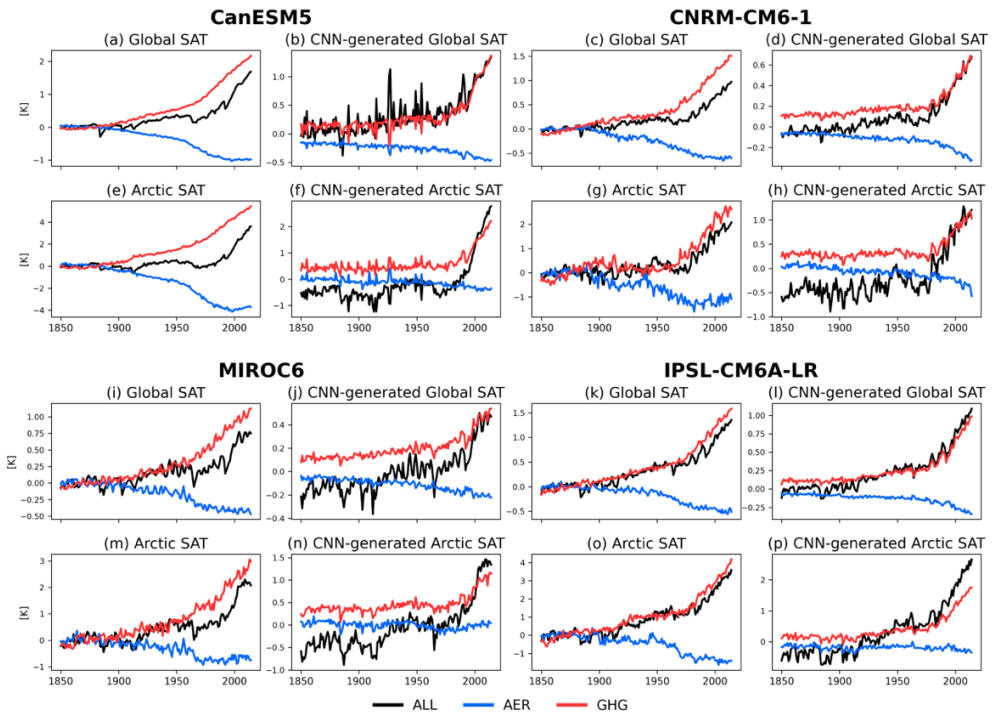

Figure 7: Panels (a), (c), (i), and (k) show the global SAT for the four models, CanESM5, CNRM-CM6-1, MIROC6, and IPSL-CM6A-LR, respectively. Panels (b), (d), (j), and (l)

doi:10.6342/NTU202404648

display the CNN-generated global SAT for the respective models. Panels (e), (g), (m), and (o) present the Arctic SAT for each of these models, while panels (f), (h), (n), and (p) represent the CNN-generated Arctic SAT.

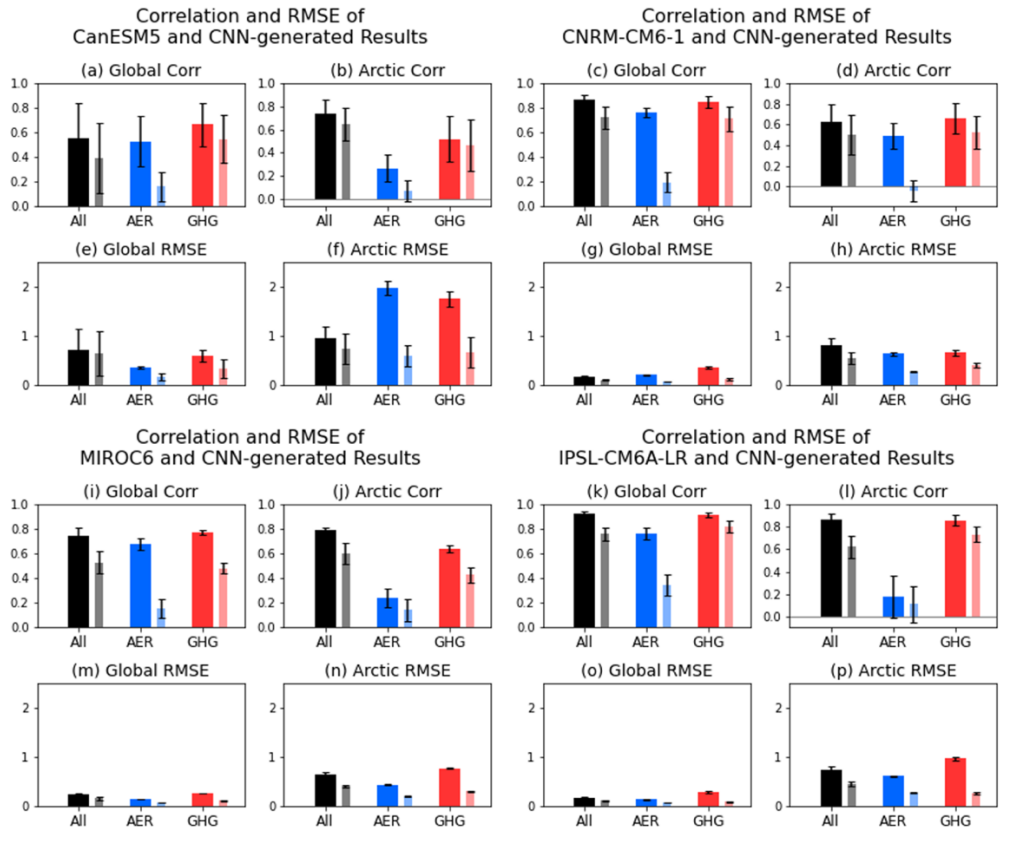

Figure 8: Panels (a) and (b) display the correlation coefficients between the annual data of the global and Arctic targets from CanESM5 and the corresponding CNN-generated results. Panels (e) and (f) show the root-mean-square error (RMSE) for the global and Arctic regions, respectively. The same structure is used for other models: panels (c), (d), (g), and (h) for CNRM-CM6-1; panels (i), (j), (m), and (n) for MIROC6; and panels (k), (l), (o), and (p) for IPSL-CM6A-LR. Error bars indicate the standard deviation across ensemble members, with thinner bars showing results after detrending.

doi:10.6342/NTU202404648

Finally, and perhaps most intriguingly, we apply the trained CNN to observational data to estimate the forced response for each of the four forcing agents. We use SAT data from the Hadley Centre (referred to as HadCRUT) because due to the higher accuracy of reanalysis data in reflecting actual atmospheric conditions, which helps to better understand and evaluate the biases present in our network model. The output global SAT time series for ALL forcings exhibits similar decadal variations to the HadCRUT time series before 1970 (Figure 9a). A warming trend becomes apparent after around 1975; however, the CESM2 SAT time series for ALL forcing overall shows smaller values than the HadCRUT SAT series. Notably, the CO2 contribution dominates, as the CO2 and ALL time series are closely aligned, which differs from the CESM2 results, while the BMB and EE contributions remain minimal. Unexpectedly, the AER time series does not exhibit the cooling trend seen in the CESM2 AER time series. Instead, the HadCRUT AER time series shows a relatively flat trajectory, suggesting that the CNN may not effectively distinguish the AER-forced signal within the observational global SAT data. For the Arctic, the estimated forced time series show similar evolution to the HadCRUT with ALL and CO2 stronger in amplitude (Figure 9b). This seems not reasonable as the Arctic SAT response tends to amplified the global SAT one.

doi:10.6342/NTU202404648

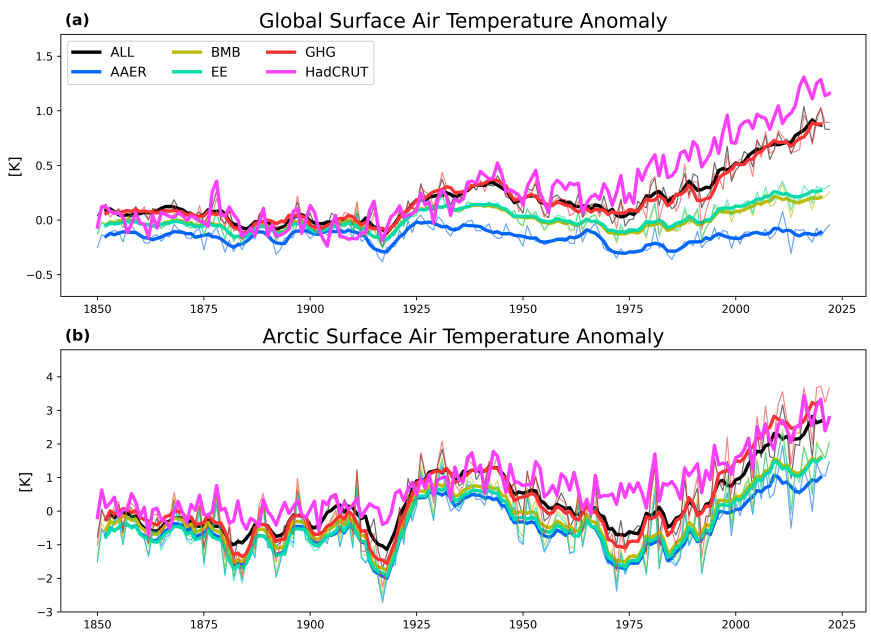

Figure 9: The annual mean data from HadCRUT are represented by a pink line. Other colors indicate the CNN-generated forcing decomposition results, with thin lines depicting the direct outputs and thick lines illustrating the smoothed results obtained using a five-year moving average.

This limitation is evident in the temporal correlation and RMSE results (Figure 9). The correlation coefficients are generally lower than in previous cases, with values for the AER and BMB cases falling below 0.2 (Figures 10a and b). In some instances, opposite signs appear, such as for the BMB global SAT and AER Arctic SAT. Additionally, the RMSE values are larger (Figures 10c and d). These results suggest that the CNN model, trained on CESM2 simulations, may not generalize effectively to observational records. We will explore possible reasons for this in future studies.

doi:10.6342/NTU202404648

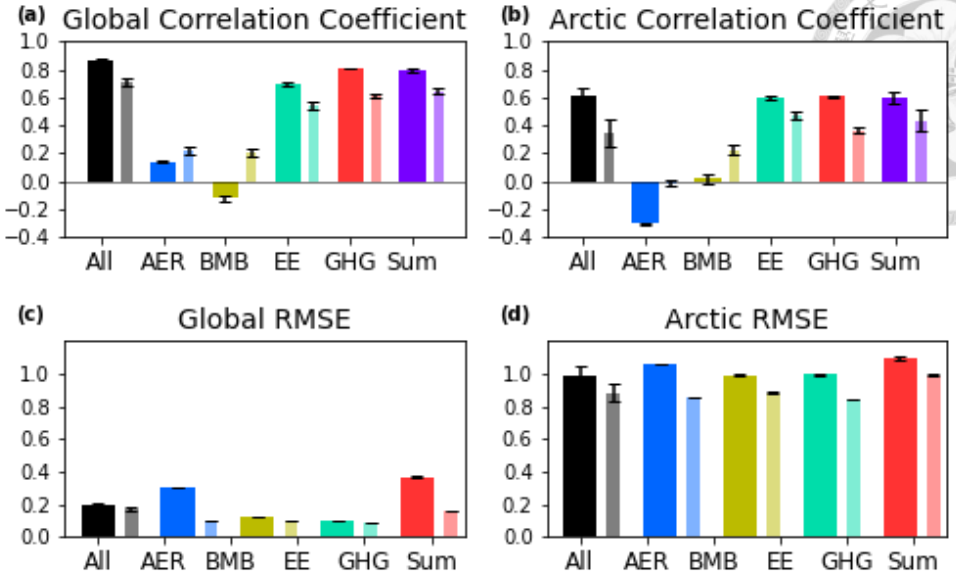

Figure 10: Correlation coefficients between the annual data of the (a) global and (b) Arctic targets from CESM2 and CNN-generated HadCRUT results. Panels (c) and (d) show the RMSE for the global and Arctic regions. Error bars represent the standard deviation across 15 ensemble members, with thinner bars indicating the results after detrending.

doi:10.6342/NTU202404648

REFERENCES

[1] Alexeev, V. A. & Jackson, C. H. (2013), 'Polar amplification: is atmospheric heat transport important?', *Climate Dynamics* 41, 533–547.

[2] Alexeev, V., Langen, P. & Bates, J. (2005), 'Polar amplification of surface warming on an aquaplanet in "ghost forcing" experiments without sea ice feedbacks', *Climate Dynamics* 24, 655–666.

[3] Armour, K. C., Bitz, C. M. & Roe, G. H. (2013), 'Time-varying climate sensitivity from regional feedbacks', *Journal of Climate* 26(13), 4518–4534.

[4] Armour, K. C., Siler, N., Donohoe, A. & Roe, G. H. (2019), 'Meridional atmospheric heat transport constrained by energetics and mediated by large-scale diffusion', *Journal of Climate* 32(12), 3655–3680.

[5] Barnes, E. A. (2013), 'Revisiting the evidence linking arctic amplification to extreme weather in midlatitudes', *Geophysical research letters* 40(17), 4734–4739.

[6] Barnes, E. A. & Screen, J. A. (2015), 'The impact of arctic warming on the midlatitude jet-stream: Can it? has it? will it?', *Wiley Interdisciplinary Reviews: Climate Change* 6(3), 277–286.

[7] Beer, E. & Eisenman, I. (2022), 'Revisiting the role of the water vapor and lapse rate feedbacks in the arctic amplification of climate change', *Journal of Climate* 35(10), 2975–2988.

[8] Blackport, R. & Kushner, P. J. (2017), 'Isolating the atmospheric circulation response to arctic sea ice loss in the coupled climate system', *Journal of Climate* 30(6), 2163–2185.

doi:10.6342/NTU202404648

[9] Blackport, R. & Screen, J. A. (2020a), 'Insignificant effect of arctic amplification on the amplitude of midlatitude atmospheric waves', *Science Advances* 6(8), eaay2880.

[10] Blackport, R. & Screen, J. A. (2020b), 'Weakened evidence for mid-latitude impacts of arctic warming', *Nature Climate Change* 10(12), 1065–1066.

[11] Blackport, R., Screen, J. A., van der Wiel, K. & Bintanja, R. (2019), 'Minimal influence of reduced arctic sea ice on coincident cold winters in mid-latitudes', *Nature Climate Change* 9(9), 697–704.

[12] Block, K. & Mauritsen, T. (2013), 'Forcing and feedback in the mpi-esm-lr coupled model under abruptly quadrupled CO2', *Journal of Advances in Modeling Earth Systems* 5(4), 676–691.

[13] Boer, G. (2011), 'The ratio of land to ocean temperature change under global warming', *Climate Dynamics* 37(11), 2253–2270.

[14] Bonan, D., Armour, K., Roe, G., Siler, N. & Feldl, N. (2018), 'Sources of uncertainty in the meridional pattern of climate change', *Geophysical Research Letters* 45(17), 91319140.

[15] Bône, C., Gastineau, G., Thiria, S., Gallinari, P. & Mejia, C. (2023), 'Detection and attribution of climate change using a neural network', *Journal of Advances in Modeling Earth Systems* 15(10), e2022MS003475.

[16] Bône, C., Gastineau, G., Thiria, S., Gallinari, P. & Mejia, C. (2024), 'Separation of internal and forced variability of climate using a u-net', *Journal of Advances in Modeling Earth Systems* 16(6), e2023MS003964.

[17] Bonnet, R., Boucher, O., Deshayes, J., Gastineau, G., Hourdin, F., Mignot, J., Servonnat, J. & Swingedouw, D. (2021), 'Presentation and evaluation of the

doi:10.6342/NTU202404648

ipslcm6a-lr ensemble of extended historical simulations', *Journal of Advances in Modeling Earth Systems* 13(9), e2021MS002565.

[18] Byrne, M. P. & O'Gorman, P. A. (2013), 'Land–ocean warming contrast over a wide range of climates: Convective quasi-equilibrium theory and idealized simulations', *Journal of Climate* 26(12), 4000–4016.

[19] Caballero, R. & Langen, P. L. (2005), 'The dynamic range of poleward energy transport in an atmospheric general circulation model', *Geophysical Research Letters* 32(2).

[20] Caesar, L., Rahmstorf, S. & Feulner, G. (2020), 'On the relationship between atlantic meridional overturning circulation slowdown and global surface warming', *Environmental Research Letters* 15(2), 024003.

[21] Cassou, C., Kushnir, Y., Hawkins, E., Pirani, A., Kucharski, F., Kang, I.-S. & Caltabiano, N. (2018), 'Decadal climate variability and predictability: Challenges and opportunities', *Bulletin of the American Meteorological Society* 99(3), 479–490.

[22] Chalmers, J., Kay, J. E., Middlemas, E. A., Maroon, E. A. & DiNezio, P. (2022), 'Does disabling cloud radiative feedbacks change spatial patterns of surface greenhouse warming and cooling?', *Journal of Climate* 35(6), 1787–1807.

[23] Chen, X., Luo, D., Wu, Y., Dunn-Sigouin, E. & Lu, J. (2021), 'Nonlinear response of atmospheric blocking to early winter barents–kara seas warming: An idealized model study', *Journal of Climate* 34(6), 2367–2383.

[24] Chen, X. & Tung, K.-K. (2014), 'Varying planetary heat sink led to global-warming slowdown and acceleration', *Science* 345(6199), 897–903.

[25] Chen, X. & Tung, K.-K. (2018), 'Global surface warming enhanced by weak atlantic overturning circulation', *Nature* 559(7714), 387–391.

doi:10.6342/NTU202404648

[26] Chiang, J. C. & Friedman, A. R. (2012), 'Extratropical cooling, interhemispheric thermal gradients, and tropical climate change', *Annual Review of Earth and Planetary Sciences* 40(1), 383–412.

[27] Chung, E.-S., Ha, K.-J., Timmermann, A., Stuecker, M. F., Bodai, T. & Lee, S.-K. (2021), 'Cold-season arctic amplification driven by arctic ocean-mediated seasonal energy transfer', *Earth's Future* 9(2), e2020EF001898.

[28] Chylek, P., Folland, C., Klett, J. D., Wang, M., Hengartner, N., Lesins, G. & Dubey, M. K. (2022), 'Annual mean arctic amplification 1970–2020: observed and simulated by cmip6 climate models', *Geophysical Research Letters* 49(13), e2022GL099371.

[29] Cohen, J., Pfeiffer, K. & Francis, J. A. (2018), 'Warm arctic episodes linked with increased frequency of extreme winter weather in the united states', *Nature Communications* 9(1), 869.

[30] Cohen, J., Screen, J. A., Furtado, J. C., Barlow, M., Whittleston, D., Coumou, D., Francis, J., Dethloff, K., Entekhabi, D., Overland, J. et al. (2014), 'Recent arctic amplification and extreme mid-latitude weather', *Nature Geoscience* 7(9), 627–637.

[31] Cohen, J., Zhang, X., Francis, J., Jung, T., Kwok, R., Overland, J., Ballinger, T., Bhatt, U., Chen, H., Coumou, D. et al. (2020), 'Divergent consensuses on arctic amplification influence on midlatitude severe winter weather', *Nature Climate Change* 10(1), 20–29.

[32] Coumou, D., Di Capua, G., Vavrus, S., Wang, L. & Wang, S. (2018), 'The influence of arctic amplification on mid-latitude summer circulation', *Nature Communications* 9(1), 2959.

doi:10.6342/NTU202404648

[33] Crook, J. A., Forster, P. M. & Stuber, N. (2011), 'Spatial patterns of modeled climate feedback and contributions to temperature response and polar amplification', *Journal of Climate* 24(14), 3575–3592.

[34] Dai, A., Huang, D., Rose, B. E., Zhu, J. & Tian, X. (2020), 'Improved methods for estimating equilibrium climate sensitivity from transient warming simulations', *Climate Dynamics* 54, 4515–4543.

[35] Dai, A., Luo, D., Song, M. & Liu, J. (2019), 'Arctic amplification is caused by sea-ice loss under increasing co2', *Nature Communications* 10(1), 121.

[36] Deser, C., Lehner, F., Rodgers, K. B., Ault, T., Delworth, T. L., DiNezio, P. N., Fiore, A., Frankignoul, C., Fyfe, J. C., Horton, D. E. et al. (2020), 'Insights from earth system model initial-condition large ensembles and future prospects', *Nature Climate Change* 10(4), 277–286.

[37] Deser, C., Phillips, A., Bourdette, V. & Teng, H. (2012), 'Uncertainty in climate change projections: the role of internal variability', *Climate Dynamics* 38, 527–546

[38] Deser, C., Phillips, A. S., Alexander, M. A. & Smoliak, B. V. (2014), 'Projecting north american climate over the next 50 years: Uncertainty due to internal variability', *Journal of Climate* 27(6), 2271–2296.

[39] Deser, C., Tomas, R. A. & Sun, L. (2015), 'The role of ocean–atmosphere coupling in the zonal-mean atmospheric response to arctic sea ice loss', *Journal of Climate* 28(6), 2168–2186.

[40] Deser, C., Tomas, R., Alexander, M. & Lawrence, D. (2010), 'The seasonal atmospheric response to projected arctic sea ice loss in the late twenty-first century', *Journal of Climate* 23(2), 333–351.

[41] Dunne, J. P., Winton, M., Bacmeister, J., Danabasoglu, G., Gettelman, A., Golaz, J.-C., Hannay, C., Schmidt, G. A., Krasting, J. P., Leung, L. R. et al. (2020),

doi:10.6342/NTU202404648

‘Comparison of equilibrium climate sensitivity estimates from slab ocean, 150-year, and longer simulations’, *Geophysical Research Letters* 47(16), e2020GL088852.

[42] Enfield, D. B. & Cid-Serrano, L. (2010), ‘Secular and multidecadal warmings in the north atlantic and their relationships with major hurricane activity’, *International Journal of Climatology: A Journal of the Royal Meteorological Society* 30(2), 174184.

[43] England, M. H., McGregor, S., Spence, P., Meehl, G. A., Timmermann, A., Cai, W., Gupta, A. S., McPhaden, M. J., Purich, A. & Santoso, A. (2014), ‘Recent intensification of wind-driven circulation in the pacific and the ongoing warming hiatus’, *Nature Climate Change* 4(3), 222–227.

[44] England, M. R., Eisenman, I., Lutsko, N. J., & Wagner, T. J. (2021), ‘The recent emergence of Arctic amplification’, *Geophysical Research Letters*, 48(15), e2021GL094086.

[45] Eyring, V., Bony, S., Meehl, G. A., Senior, C. A., Stevens, B., Stouffer, R. J. & Taylor, K. E. (2016), ‘Overview of the coupled model intercomparison project phase 6 (cmip6) experimental design and organization’, *Geoscientific Model Development* 9(5), 19371958.

[46] Eyring, V., Gillett, N. P., Achuta Rao, K. M., Barimalala, R., Barreiro Parrillo, M., Bellouin, N., Cassou, C., Durack, P. J., Kosaka, Y., McGregor, S. et al. (2021), ‘Human influence on the climate system (chapter 3)’.

[47] Fabiano, F., Davini, P., Meccia, V. L., Zappa, G., Bellucci, A., Lembo, V., Bellomo, K. & Corti, S. (2024), ‘Multi-centennial evolution of the climate response and deep-ocean heat uptake in a set of abrupt stabilization scenarios with ec-earth3’, *Earth System Dynamics* 15(2), 527–546.

doi:10.6342/NTU202404648

[48] Fan, Y., Liu, W., Zhang, P., Chen, R. & Li, L. (2023), 'North atlantic oscillation contributes to the subpolar north atlantic cooling in the past century', *Climate Dynamics* 61(11), 5199–5215.

[49] Feichter, J., Roeckner, E., Lohmann, U. & Liepert, B. (2004), 'Nonlinear aspects of the climate response to greenhouse gas and aerosol forcing', *Journal of Climate* 17(12), 2384–2398.

[50] Feldl, N., Bordoni, S. & Merlis, T. M. (2017), 'Coupled high-latitude climate feedbacks and their impact on atmospheric heat transport', *Journal of Climate* 30(1), 189–201.

[51] Feldl, N., Po-Chedley, S., Singh, H. K., Hay, S. & Kushner, P. J. (2020), 'Sea ice and atmospheric circulation shape the high-latitude lapse rate feedback', *Npj Climate and Atmospheric Science* 3(1), 41.

[52] Francis, J. A. & Vavrus, S. J. (2012), 'Evidence linking arctic amplification to extreme weather in mid-latitudes', *Geophysical Research Letters* 39(6).

[53] Francis, J. & Skific, N. (2015), 'Evidence linking rapid arctic warming to mid-latitude weather patterns', *Philosophical Transactions of the Royal Society A: Mathematical, Physical and Engineering Sciences* 373(2045), 20140170.

[54] Frankcombe, L. M., England, M. H., Mann, M. E. & Steinman, B. A. (2015), 'Separating internal variability from the externally forced climate response', *Journal of Climate* 28(20), 8184–8202.

[55] Frankignoul, C., Gastineau, G. & Kwon, Y.-O. (2017), 'Estimation of the sst response to anthropogenic and external forcing and its impact on the atlantic multidecadal oscillation and the pacific decadal oscillation', *Journal of Climate* 30(24), 9871–9895.

doi:10.6342/NTU202404648

[56] Gillett, N. P., Stone, D. A., Stott, P. A., Nozawa, T., Karpechko, A. Y., Hegerl, G. C., Wehner, M. F. & Jones, P. D. (2008), 'Attribution of polar warming to human influence', *Nature Geoscience* 1(11), 750–754.

[57] Goosse, H., Kay, J. E., Armour, K. C., Bodas-Salcedo, A., Chepfer, H., Docquier, D., Jonko, A., Kushner, P. J., Lecomte, O., Massonnet, F. et al. (2018), 'Quantifying climate feedbacks in polar regions', *Nature Communications* 9(1), 1919.

[58] Graversen, R. G., Langen, P. L. & Mauritsen, T. (2014), 'Polar amplification in ccsm4: Contributions from the lapse rate and surface albedo feedbacks', *Journal of Climate* 27(12), 4433–4450.

[59] Graversen, R. G. & Wang, M. (2009), 'Polar amplification in a coupled climate model with locked albedo', *Climate Dynamics* 33, 629–643.

[60] Hahn, L. C., Armour, K. C., Zelinka, M. D., Bitz, C. M. & Donohoe, A. (2021), 'Contributions to polar amplification in cmip5 and cmip6 models', F*rontiers in Earth Science* 9, 710036.

[61] Hall, A. (2004), 'The role of surface albedo feedback in climate', *Journal of Climate* 17(7), 1550–1568.

[62] Ham, Y.-G., Kim, J.-H., Min, S.-K., Kim, D., Li, T., Timmermann, A. & Stuecker, M. F. (2023), 'Anthropogenic fingerprints in daily precipitation revealed by deep learning', *Nature* 622(7982), 301–307.

[63] Harzallah, A. & Sadourny, R. (1995), 'Internal versus sst-forced atmospheric variability as simulated by an atmospheric general circulation model', *Journal of Climate* 8(3), 474–495.

[64] Hawkins, E. & Sutton, R. (2009), 'The potential to narrow uncertainty in regional climate predictions', *Bulletin of the American Meteorological Society* 90(8), 10951108.

doi:10.6342/NTU202404648

[65] Henry, M. & Merlis, T. M. (2019), 'The role of the nonlinearity of the stefan–boltzmann law on the structure of radiatively forced temperature change', *Journal of Climate* 32(2), 335–348.

[66] Hoffert, M. I. & Covey, C. (1992), 'Deriving global climate sensitivity from palaeoclimate reconstructions', *Nature* 360(6404), 573–576.

[67] Hu, X., Liu, Y., Kong, Y. & Yang, Q. (2022), 'A quantitative analysis of the source of inter-model spread in arctic surface warming response to increased CO2 concentration', *Geophysical Research Letters* 49(18), e2022GL100034.

[68] Hwang, Y.-T. & Frierson, D. M. (2010), 'Increasing atmospheric poleward energy transport with global warming', *Geophysical Research Letters* 37(24).

[69] Hwang, Y.-T., Frierson, D. M. & Kay, J. E. (2011), 'Coupling between arctic feedbacks and changes in poleward energy transport', *Geophysical Research Letters* 38(17).

[70] Jansen, M. F. (2017), 'Glacial ocean circulation and stratification explained by reduced atmospheric temperature', *Proceedings of the National Academy of Sciences* 114(1), 45–50.

[71] Jeffrey, S., Rotstayn, L., Collier, M., Dravitzki, S., Hamalainen, C., Moeseneder, C., Wong, K. & Syktus, J. (2013), 'Australia's cmip5 submission usingthe csiro-mk3. 6 model', *Australian Meteorological and Oceanographic Journal* 63(1), 1–13.

[72] Jenkins, M. & Dai, A. (2021), 'The impact of sea-ice loss on arctic climate feedbacks and their role for arctic amplification', *Geophysical Research Letters* 48(15), e2021GL094599.

[73] Jiang, Y., Yang, X.-Q., Liu, X., Qian, Y., Zhang, K., Wang, M., Li, F., Wang, Y. & Lu, Z. (2020), 'Impacts of wildfire aerosols on global energy budget and climate: The role of climate feedbacks', *Journal of Climate* 33(8), 3351–3366.

doi:10.6342/NTU202404648

[74] Jones, G. S., Stott, P. A. & Christidis, N. (2013), 'Attribution of observed historical near–surface temperature variations to anthropogenic and natural causes using cmip5 simulations', *Journal of Geophysical Research: Atmospheres* 118(10), 4001–4024.

[75] Jonko, A. K., Shell, K. M., Sanderson, B. M. & Danabasoglu, G. (2013), 'Climate feedbacks in ccsm3 under changing co 2 forcing. part ii: Variation of climate feedbacks and sensitivity with forcing', *Journal of Climate* 26(9), 2784–2795.

[76] Joshi, M. M., Gregory, J. M., Webb, M. J., Sexton, D. M. & Johns, T. C. (2008), 'Mechanisms for the land/sea warming contrast exhibited by simulations of climate change', *Climate dynamics* 30, 455–465.

[77] Kay, J. E., Deser, C., Phillips, A., Mai, A., Hannay, C., Strand, G., Arblaster, J. M., Bates, S., Danabasoglu, G., Edwards, J. et al. (2015), 'The Community Earth System Model (CESM) large ensemble project: A community resource for studying climate change in the presence of internal climate variability', *Bulletin of the American Meteorological Society* 96(8), 1333–1349.

[78] Kay, J. E., Liang, Y.-C., Zhou, S.-N. & Maher, N. (2024), 'Sea ice feedbacks cause more greenhouse cooling than greenhouse warming at high northern latitudes on multicentury timescales', *Environmental Research: Climate* 3(4), 041003.

[79] Kosaka, Y. & Xie, S.-P. (2013), 'Recent global-warming hiatus tied to equatorial pacific surface cooling', *Nature* 501(7467), 403–407.

[80] Kug, J.-S., Jeong, J.-H., Jang, Y.-S., Kim, B.-M., Folland, C. K., Min, S.-K. & Son, S.-W. (2015), 'Two distinct influences of arctic warming on cold winters over north america and east asia', *Nature Geoscience* 8(10), 759–762.

doi:10.6342/NTU202404648

[81] Kumar, A., Yadav, J. & Mohan, R. (2021), 'Spatio-temporal change and variability of barents-kara sea ice, in the arctic: Ocean and atmospheric implications', *Science of The Total Environment* 753, 142046.

[82] Langen, P. L., Graversen, R. G. & Mauritsen, T. (2012), 'Separation of contributions from radiative feedbacks to polar amplification on an aquaplanet', *Journal of Climate* 25(8), 3010–3024.

[83] Lenssen, N. J., Schmidt, G. A., Hansen, J. E., Menne, M. J., Persin, A., Ruedy, R. & Zyss, D. (2019), 'Improvements in the gistemp uncertainty model', *Journal of Geophysical Research: Atmospheres* 124(12), 6307–6326.

[84] Liang, Y.-C., Polvani, L. M. & Mitevski, I. (2022a), 'Arctic amplification, and its seasonal migration, over a wide range of abrupt co2 forcing', *Npj Climate and Atmospheric Science* 5(1), 14.

[85] Liang, Y.-C., Polvani, L. M., Previdi, M., Smith, K. L., England, M. R. & Chiodo, G. (2022b), 'Stronger arctic amplification from ozone-depleting substances than from carbon dioxide', *Environmental Research Letters* 17(2), 024010.

[86] Long, D. J. & Collins, M. (2013), 'Quantifying global climate feedbacks, responses and forcing under abrupt and gradual co 2 forcing', *Climate Dynamics* 41, 2471–2479.

[87] Ma, J., Xie, S.-P. & Kosaka, Y. (2012), 'Mechanisms for tropical tropospheric circulation change in response to global warming', *Journal of Climate* 25(8), 2979–2994.

[88] Manabe, S. & Wetherald, R. T. (1975), 'The effects of doubling the co 2 concentration on the climate of a general circulation model', *Journal of Atmospheric Sciences* 32(1), 315.

doi:10.6342/NTU202404648

[89] Mauritsen, T., Graversen, R. G., Klocke, D., Langen, P. L., Stevens, B. & Tomassini, L. (2013), 'Climate feedback efficiency and synergy', *Climate Dynamics* 41, 2539–2554.

[90] Meehl, G. A., Hu, A., Arblaster, J. M., Fasullo, J. & Trenberth, K. E. (2013), 'Externally forced and internally generated decadal climate variability associated with the interdecadal pacific oscillation', *Journal of Climate* 26(18), 7298–7310.

[91] Meredith, M. P., Sommerkorn, M., Cassotta, S., Derksen, C., Ekaykin, A. A., Hollowed, A. B., Kofinas, G., Mackintosh, A. N., Muelbert, M. M. C., Melbourne-Thomas, J. et al. (2019), 'Polar regions', in *The Ocean and Cryosphere in a Changing Climate: Summary for Policymakers*, Intergovernmental Panel on Climate Change, pp. 3–1.

[92] Middlemas, E., Kay, J., Medeiros, B. & Maroon, E. (2020), 'Quantifying the influence of cloud radiative feedbacks on arctic surface warming using cloud locking in an earth system model', *Geophysical Research Letters* 47(15), e2020GL089207.

[93] Miller, G. H., Alley, R. B., Brigham-Grette, J., Fitzpatrick, J. J., Polyak, L., Serreze, M. C. & White, J. W. (2010), 'Arctic amplification: can the past constrain the future?', *Quaternary Science Reviews* 29(15-16), 1779–1790.

[94] Ming, Y. & Ramaswamy, V. (2009), 'Nonlinear climate and hydrological responses to aerosol effects', *Journal of Climate* 22(6), 1329–1339.

[95] Mitevski, I., Orbe, C., Chemke, R., Nazarenko, L. & Polvani, L. M. (2021), 'Non-monotonic response of the climate system to abrupt CO2 forcing', *Geophysical Research Letters* 48, e2020GL090861.

doi:10.6342/NTU202404648

[96] Mitevski, I., Polvani, L. M. & Orbe, C. (2022), 'Asymmetric warming/cooling response to CO2 increase/decrease mainly due to non-logarithmic forcing, not feedbacks', *Geophysical Research Letters* 49, e2021GL097133.

[97] Mori, M., Watanabe, M., Shiogama, H., Inoue, J. & Kimoto, M. (2014), 'Robust Arctic sea-ice influence on the frequent Eurasian cold winters in past decades', *Nature Geoscience* 7, 869–873.

[98] Newman, M., Alexander, M. A., Ault, T. R., Cobb, K. M., Deser, C., Di Lorenzo, E., Mantua, N. J., Miller, A. J., Minobe, S., & Nakamura, H. (2016). 'The Pacific Decadal Oscillation, Revisited.' *Journal of Climate*, 29(12), 4399–4427.

[99] Oudar, T., Sanchez-Gomez, E., Chauvin, F., Cattiaux, J., Terray, L. & Cassou, C. (2017), 'Respective roles of direct GHG radiative forcing and induced Arctic sea ice loss on the northern hemisphere atmospheric circulation', *Climate Dynamic*s 49, 3693–3713.

[100] Overland, J. E., Dethloff, K., Francis, J. A., Hall, R. J., Hanna, E., Kim, S.-J., Screen, J. A., Shepherd, T. G. & Vihma, T. (2016), 'Nonlinear response of mid-latitude weather to the changing Arctic', *Nature Climate Change* 6, 992–9.

[101] Overland, J., Francis, J. A., Hall, R., Hanna, E., Kim, S.-J. & Vihma, T. (2015), 'The melting Arctic and midlatitude weather patterns: are they connected?', *Journal of Climate* 28, 7917–32.

[102] Palter, J. B. (2015), 'The role of the gulf stream in European climate', *Annual Review of Marine Science* 7, 113–137.

[103] Pendergrass, A. G., Conley, A. & Vitt, F. M. (2018), 'Surface and top-of-atmosphere radiative feedback kernels for CESM-CAM5', *Earth System Science Data* 10(1), 317–324.

doi:10.6342/NTU202404648

[104] Penland, C. & Matrosova, L. (1994). 'A balance condition for stochastic numerical models with application to the El Niño–Southern Oscillation.' *Journal of Climate*, 7(9), 1352–1372.

[105] Penland, C. & Matrosova, L. (2006). 'Studies of El Niño and interdecadal variability in tropical sea surface temperatures using a nonnormal filter.' *Journal of Climate*, 19(22), 5796–5815.

[106] Pithan, F. & Mauritsen, T. (2014), 'Arctic amplification dominated by temperature feedbacks in contemporary climate models', *Nature geoscience* 7, 181–4.

[107] Polvani, L. M., Previdi, M., England, M. R., Chiodo, G. & Smith, K. L. (2020), 'Substantial twentieth-century Arctic warming caused by ozone-depleting substances', *Nature Climate Change* 10(2), 130–133.

[108] Previdi, M., Polvani, L. M., Smith, K. L. & Wills, R. C. J. (2020), 'Arctic amplification: A rapid response to radiative forcing', *Geophysical Research Letters* 47(17), e2020GL089933.

[109] Rantanen, Mika, et al. (2022), 'The Arctic has warmed nearly four times faster than the globe since 1979'. *Communications Earth & Environment 3*(1), 168.

[110] Rodgers, K. B., Lin, J., & Frölicher, T. L. (2015). 'Emergence of multiple ocean ecosystem drivers in a large ensemble suite with an Earth system model.' *Biogeosciences* 12(11), 3301–3320.

[111] Roe, G. H. & Baker, M. B. (2007), 'Why is climate sensitivity so unpredictable?', *Science* 318(5850), 629–632.

[112] Roe, G. H., Feldl, N., Armour, K. C., Hwang, Y.-T. & Frierson, D. M. W. (2015), 'The remote impacts of climate feedbacks on regional climate predictability', *Nature Geoscience* 8(2), 135–139.

doi:10.6342/NTU202404648

[113] Rose, B. E. J., Armour, K. C., Battisti, D. S., Feldl, N. & Koll, D. D. B. (2014), 'The dependence of transient climate sensitivity and radiative feedbacks on the spatial pattern of ocean heat uptake', *Geophysical Research Letters* 41(4), 1071–1078.

[114] Rugenstein, M. A. A., Sedláček, J. & Knutti, R. (2016), 'Nonlinearities in patterns of long-term ocean warming', *Geophysical Research Letters* 43(7), 3380–3388.

[115] Rugenstein, M. A. A., Winton, M., Stouffer, R. J., Griffies, S. M. & Hallberg, R. (2013), 'Northern high-latitude heat budget decomposition and transient warming', *Journal of Climate* 26(2), 609–621.

[116] Rugenstein, M. et al. (2020), 'Equilibrium climate sensitivity estimated by equilibrating climate models', *Geophysical Research Letters* 47(4), e2019GL083898.

[117] Russotto, R. D. & Biasutti, M. (2020), 'Polar amplification as an inherent response of a circulating atmosphere: results from the tracmip aquaplanets', *Geophysical Research Letters* 47, e2019GL086771.

[118] Schmidt, A., Mills, M. J., Ghan, S., Gregory, J. M., Allan, R. P., Andrews, T., Forster, P. M., Jones, A., Kravitz, B., Lamb, K., Mann, G. W., Marshall, L., & Robock, A. (2018). 'Volcanic Radiative Forcing From 1979 to 2015.' *Journal of Geophysical Research: Atmospheres*, 123(22), 12,491–12,508.

[119] Screen, J. A. & Simmonds, I. (2010), 'Increasing fall-winter energy loss from the arctic ocean and its role in arctic temperature amplification', *Geophysical research letters* 37(16).

[120] Serreze, M. C., Barrett, A., Stroeve, J., Kindig, D. & Holland, M. (2009), 'The emergence of surface-based arctic amplification', *The Cryosphere* 3(1), 11–19.

[121] Serreze, M. C. & Francis, J. A. (2006), 'The arctic amplification debate', *Climatic Change* 76(3), 241–264.

doi:10.6342/NTU202404648

[122] Sévellec, F., Fedorov, A. V. & Liu, W. (2017), 'Arctic sea-ice decline weakens the atlantic meridional overturning circulation', *Nature Climate Change* 7(8), 604–610.

[123] Smith, D. M., Eade, R., Andrews, M., Ayres, H., Clark, A., Chripko, S., Deser, C., Dunstone, N., García-Serrano, J., Gastineau, G. et al. (2022), 'Robust but weak winter atmospheric circulation response to future arctic sea ice loss', *Nature Communications* 13(1), 727.

[124] Soden, B. J., Held, I. M., Colman, R., Shell, K. M., Kiehl, J. T. & Shields, C. A. (2008), 'Quantifying climate feedbacks using radiative kernels', *Journal of Climate* 21(14), 3504–3520.

[125] Solomon, S., Daniel, J. S., Neely III, R. R., Vernier, J.-P., Dutton, E. G. & Thomason, L. W. (2011), 'The persistently variable "background" stratospheric aerosol layer and global climate change', *Science* 333(6044), 866–870.

[126] Stouffer, R., Weaver, A. & Eby, M. (2004), 'A method for obtaining pre-twentieth century initial conditions for use in climate change studies', *Climate Dynamics* 23, 327–339.

[127] Stuecker, M. F., Bitz, C. M., Armour, K. C., Proistosescu, C., Kang, S. M., Xie, S.P., Kim, D., McGregor, S., Zhang, W., Zhao, S. et al. (2018), 'Polar amplification dominated by local forcing and feedbacks', *Nature Climate Change* 8(12), 1076–1081.

[128] Sumata, H., de Steur, L., Divine, D. V., Granskog, M. A. & Gerland, S. (2023), 'Regime shift in arctic ocean sea ice thickness', *Nature* 615(7952), 443–449.

[129] Swart, N. C., Fyfe, J. C., Hawkins, E., Kay, J. E. & Jahn, A. (2015), 'Influence of internal variability on arctic sea-ice trends', *Nature Climate Change* 5(2), 86–89.

doi:10.6342/NTU202404648

[130] Sweeney, A. J., Fu, Q., Po-Chedley, S., Wang, H. & Wang, M. (2023), 'Internal variability increased arctic amplification during 1980–2022', *Geophysical Research Letters* 50(24), e2023GL106060.

[131] Taylor, P. C., Boeke, R. C., Boisvert, L. N., Feldl, N., Henry, M., Huang, Y., Langen, P. L., Liu, W., Pithan, F., Sejas, S. A. et al. (2022), 'Process drivers, inter-model spread, and the path forward: A review of amplified arctic warming', *Frontiers in Earth Science* 9, 758361.

[132] Ting, M., Kushnir, Y., Seager, R. & Li, C. (2009), 'Forced and internal twentieth-century sst trends in the north atlantic', *Journal of Climate* 22(6), 1469–1481.

[133] Trenberth, K. E. & Shea, D. J. (2006), 'Atlantic hurricanes and natural variability in 2005', *Geophysical Research Letters* 33(12).

[134] Trossman, D., Palter, J., Merlis, T., Huang, Y. & Xia, Y. (2016), 'Large-scale ocean circulation-cloud interactions reduce the pace of transient climate change', *Geophysical Research Letters* 43(8), 3935–3943.

[135] Vallis, G. K., Zurita-Gotor, P., Cairns, C. & Kidston, J. (2015), 'Response of the largescale structure of the atmosphere to global warming', *Quarterly Journal of the Royal Meteorological Society* 141(690), 1479–1501.

[136] Vavrus, S. J. (2018), 'The influence of arctic amplification on mid-latitude weather and climate', *Current Climate Change Reports* 4, 238–249.

[137] Vincent, L. A., Zhang, X., Brown, R., Feng, Y., Mekis, E., Milewska, E., Wan, H. & Wang, X. (2015), 'Observed trends in canada's climate and influence of low-frequency variability modes', *Journal of Climate* 28(11), 4545–4560.

[138] Wang, C., Deser, C., Yu, J.-Y., DiNezio, P. & Clement, A. (2017), 'El Niño and Southern Oscillation (ENSO): A review', *Coral Reefs of the Eastern Tropical Pacific: Persistence and Loss in a Dynamic Environment,* Springer, pp. 85–106.

doi:10.6342/NTU202404648

[139] Wang, C. & Picaut, J. (2004), 'Understanding ENSO physics—a review', in *Earth's Climate: The Ocean–Atmosphere Interaction, Geophysical Monograph* 147, American Geophysical Union, pp. 21–48.

[140] Winton, M., Griffies, S. M., Samuels, B. L., Sarmiento, J. L. & Frölicher, T. L. (2013), 'Connecting changing ocean circulation with changing climate', *Journal of Climate* 26(7), 2268–2278.

[141] Wu, Y.-T., Liang, Y.-C., Kuo, Y.-N., Lehner, F., Previdi, M., Polvani, L. M., Lo, M.H. & Lan, C.-W. (2023), 'Exploiting smiles and the cmip5 archive to understand arctic climate change seasonality and uncertainty', *Geophysical Research Letters* 50(2), e2022GL100745.

[142] Yang, H. & Zhu, J. (2011), 'Equilibrium thermal response timescale of global oceans', *Geophysical Research Letters* 38(14).

[143] Zappa, G., Ceppi, P. & Shepherd, T. G. (2021), 'Eurasian cooling in response to arctic sea-ice loss is not proved by maximum covariance analysis', *Nature Climate Change* 11(2), 106–108.

[144] Zeiler, M. (2014), Visualizing and understanding convolutional networks, in 'European conference on computer vision/arXiv', Vol. 1311.

[145] Zhang, R., Sutton, R., Danabasoglu, G., Kwon, Y.-O., Marsh, R., Yeager, S. G., Amrhein, D. E. & Little, C. M. (2019), 'A review of the role of the atlantic meridional overturning circulation in atlantic multidecadal variability and associated climate impacts', *Reviews of Geophysics* 57(2), 316–375.

[146] Zhong, L., Hua, L. & Luo, D. (2018), 'Local and external moisture sources for the arctic warming over the barents–kara seas', *Journal of Climate* 31(5), 1963–1982.

doi:10.6342/NTU202404648

[147] Zhou, S.-N., Liang, Y.-C., Mitevski, I. & Polvani, L. M. (2023), 'Stronger arctic amplification produced by decreasing, not increasing, co2 concentrations', *Environmental Research: Climate* 2(4), 045001.

doi:10.6342/NTU202404648